



Article

Synthesis, In Silico Prediction and In Vitro Evaluation of Antimicrobial Activity, DFT Calculation and Theoretical Investigation of Novel Xanthenes and Uracil Containing Imidazolone Derivatives

Samar El-Kalyoubi ^{1,*} , Fatimah Agili ², Wael A. Zordok ³ and Ashraf S. A. El-Sayed ⁴

¹ Department of Pharmaceutical Organic Chemistry, Faculty of Pharmacy (Girls), Al-Azhar University, Nasr City, Cairo 11651, Egypt

² Chemistry Department, Faculty of Science (Female Section), Jazan University, Jazan 82621, Saudi Arabia; fatmah2000@gmail.com

³ Department of Chemistry, Faculty of Science, Zagazig University, Zagazig 44519, Egypt; wazordok@zu.edu.eg

⁴ Enzymology and Fungal Biotechnology, Botany and Microbiology Department, Faculty of Science, Zagazig University, Zagazig 44519, Egypt; ash.elsayed@gmail.com

* Correspondence: s.elkalyoubi@hotmail.com; Tel.: +20-111-995-2620



Citation: El-Kalyoubi, S.; Agili, F.; Zordok, W.A.; El-Sayed, A.S.A. Synthesis, In Silico Prediction and In Vitro Evaluation of Antimicrobial Activity, DFT Calculation and Theoretical Investigation of Novel Xanthenes and Uracil Containing Imidazolone Derivatives. *Int. J. Mol. Sci.* **2021**, *22*, 10979. <https://doi.org/10.3390/ijms222010979>

Academic Editors: Josef Jampilek and Miloš Hricovini

Received: 9 September 2021

Accepted: 5 October 2021

Published: 12 October 2021

Publisher's Note: MDPI stays neutral with regard to jurisdictional claims in published maps and institutional affiliations.



Copyright: © 2021 by the authors. Licensee MDPI, Basel, Switzerland. This article is an open access article distributed under the terms and conditions of the Creative Commons Attribution (CC BY) license (<https://creativecommons.org/licenses/by/4.0/>).

Abstract: Novel xanthine and imidazolone derivatives were synthesized based on oxazolone derivatives **2a-c** as a key intermediate. The corresponding xanthine **3-5** and imidazolone derivatives **6-13** were obtained via reaction of oxazolone derivative **2a-c** with 5,6-diaminouracils **1a-e** under various conditions. Xanthine compounds **3-5** were obtained by cyclocondensation of 5,6-diaminouracils **1a-c** with different oxazolones in glacial acetic acid. Moreover, 5,6-diaminouracils **1a-e** were reacted with oxazolones **2a-c** in presence of drops of acetic acid under fused condition yielding the imidazolone derivatives **6-13**. Furthermore, Schiff base of compounds **14-16** were obtained by condensing 5,6-diaminouracils **1a,b,e** with 4-dimethylaminobenzaldehyde in acetic acid. The structural identity of the resulting compounds was resolved by IR, ¹H-, ¹³C-NMR and Mass spectral analyses. The novel synthesized compounds were screened for their antifungal and antibacterial activities. Compounds **3**, **6**, **13** and **16** displayed the highest activity against *Escherichia coli* as revealed from the IC₅₀ values (1.8–1.9 µg/mL). The compound **16** displayed a significant antifungal activity against *Candida albicans* (0.82 µg/mL), *Aspergillus flavus* (1.2 µg/mL) comparing to authentic antibiotics. From the TEM microgram, the compounds **3**, **12**, **13** and **16** exhibited a strong deformation to the cellular entities, by interfering with the cell membrane components, causing cytosol leakage, cellular shrinkage and irregularity to the cell shape. In addition, docking study for the most promising antimicrobial tested compounds depicted high binding affinity against acyl carrier protein domain from a fungal type I polyketide synthase (ACP), and Baumannii penicillin-binding protein (PBP). Moreover, compound **12** showed high drug-likeness, and excellent pharmacokinetics, which needs to be in focus for further antimicrobial drug development. The most promising antimicrobial compounds underwent theoretical investigation using DFT calculation.

Keywords: oxazolone; xanthine; 5,6-diaminouracil; imidazolone; schiff base; DFT calculation; antimicrobial; molecular docking

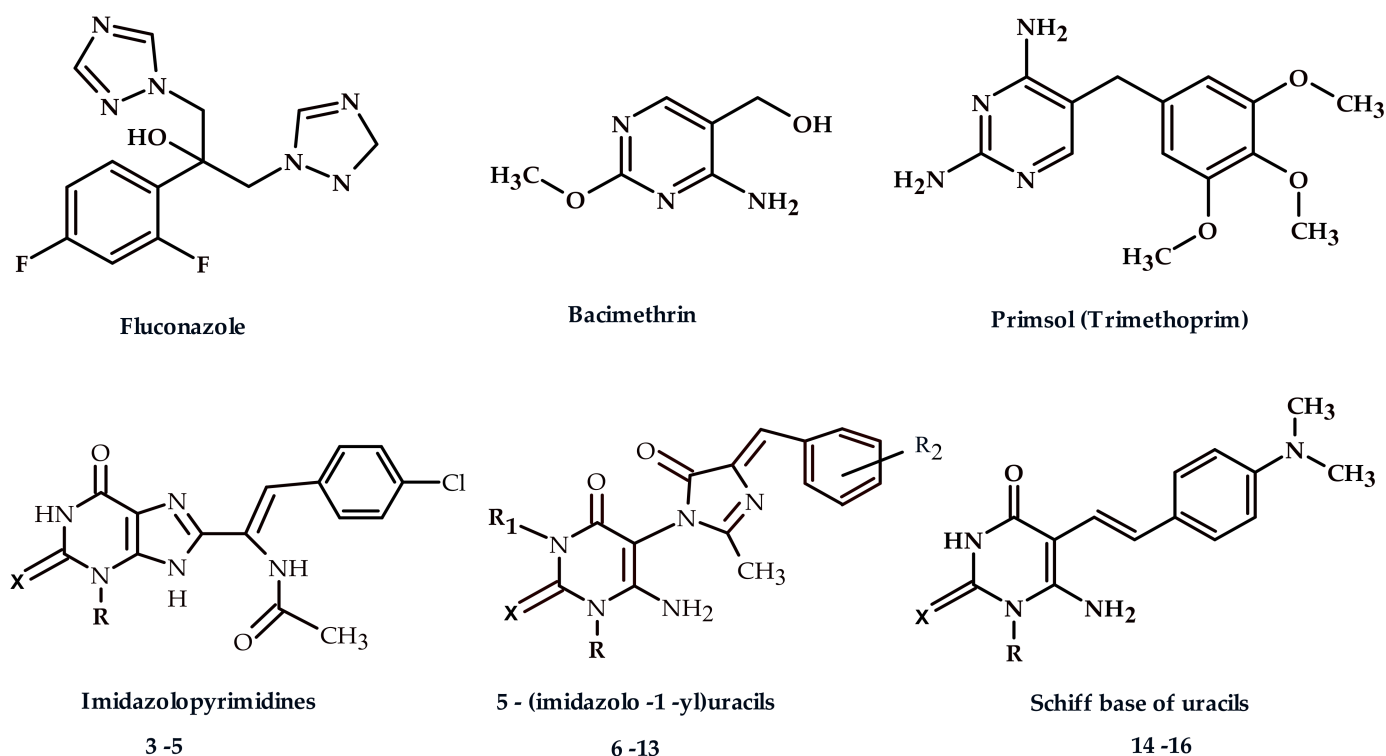
1. Introduction

Increasing the incidence of microbial resistance to antibiotics due to the overuse and misuse of antimicrobial drugs is the major challenge for controlling the pathogenic bacteria. Recently, the World Health Organization reported that excessive use of antibiotics during the COVID-19 pandemic, as well as previous H₁N₁ influenza pandemics, increased the incidence of antimicrobial resistance [1–3]. Also, the infections by antibiotic-resistant bacteria has been exceeded that of tuberculosis, HIV infections and influenza combined [4,5].

As a result, patients of chronic diseases, cancer, organ transplantation, or other reasons are at the greatest risk of infection “difficult-to-treat” caused by antibiotic-resistant bacteria. Moreover, secondary bacterial infections are common in hospitalized patients, which can significantly worsen their prognosis [6–8], where it was revealed that one out of four patients had secondary bacterial infections [4,9].

In the last century, nitrogen-based heterocycles such as various imidazole-containing compounds have been implemented in clinical trials for their antimicrobial activity and treatment of variety of diseases. The rapid expansion of imidazole-based medicinal chemistry reveals the therapeutic potential of imidazole-derivatives in treatment of various incurable diseases. Comparison to other heterocyclic rings, the imidazole core scaffold has three carbon and two nitrogen atoms with electronic-rich characteristics with higher feasibility to bind with a variety of proteins and enzyme receptors, displaying strong broad spectrum biological activities such as anti-inflammatory and anticancer activities [1,2]. The antimicrobial activity of these imidazole containing compounds elaborates from their efficiency to cause DNA double-stranded break and inhibition of protein kinase. Moreover, the anti-inflammatory mechanisms of imidazole derivatives include inhibition of COX-2 enzyme, inhibition of neutrophils degranulation, and generation of reactive oxygen species [1,2]. The imidazole ring’s structural characteristics help to generate numerous drug–ligand interactions through van der Waals forces, hydrogen bonds and hydrophobic forces [10]. Furthermore, the imidazole core scaffold is naturally found in a variety of compounds, including histidine, histamine, alkaloids, biotin and nucleic acids and several FDA-approved medication classes [4]. Fused imidazole derivatives played a significant role in medicine due to their vital medical uses. Currently, the commercial imidazole derivatives with antimicrobial, anticancer and antiinflammatory activity are metronidazole, methotrexate and omeprazole, respectively [1]. Imidazolone derivatives are the most commonly exploited bioactive heterocycles. Functionalized imidazolones were recognized by their strong therapeutic effect, especially as a powerful CNS depressant, anticonvulsant, sedative and hypnotic, fungicidal, antibacterial, antihistamine, anti-inflammatory, MAO inhibitory, antihypertensive, antiparkinsonian and anthelmintic activities [4–9,11–25].

Uracils and their derivatives are one of the most essential structural motifs for drug design [26]. The thymidine phosphorylase inhibitory action of substituted uracils at positions N1, N3, C5, and C6 is well recognized. They displayed a wide spectrum activity including antimicrobial activities [27–30], antiviral [31–33] and anticancer potency [34,35]. As well as, the acyclic and macrocyclic uracil derivatives with quaternized nitrogen exhibited a significant antibacterial and antifungal [36]. Interestingly, uracil derivatives were recognized as potent anticancer inhibitors by inhibiting histone deacetylase [37]. Based on this fact, new antimicrobial drugs will be needed to overcome these problems. Our strategy is directed towards synthesis of new compounds with potential activity against multidrug resistant Gram positive, and negative bacteria, in addition to human pathogenic fungi. The authentic drugs and the current synthesized compounds are showed in Scheme 1.

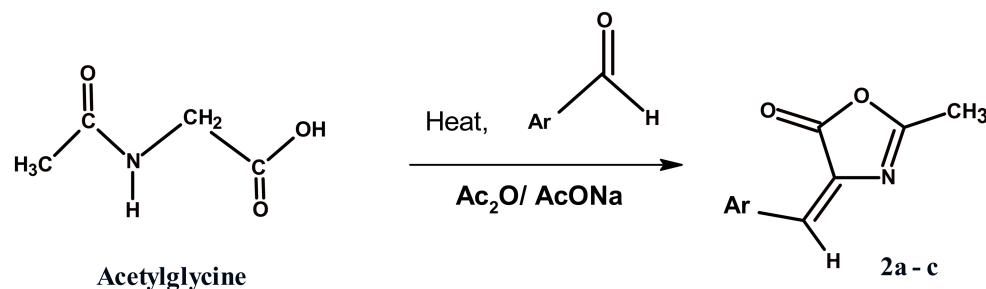


Scheme 1. Chemical structures of Fluconazole, Bacimethrin, and Primsol, as authentic drugs, and the current synthesized compounds “imidazolopyrimidine-2,4-diones, 5-(imidazole-1-yl) uracils and Schiff base of uracils.

2. Results and Discussion

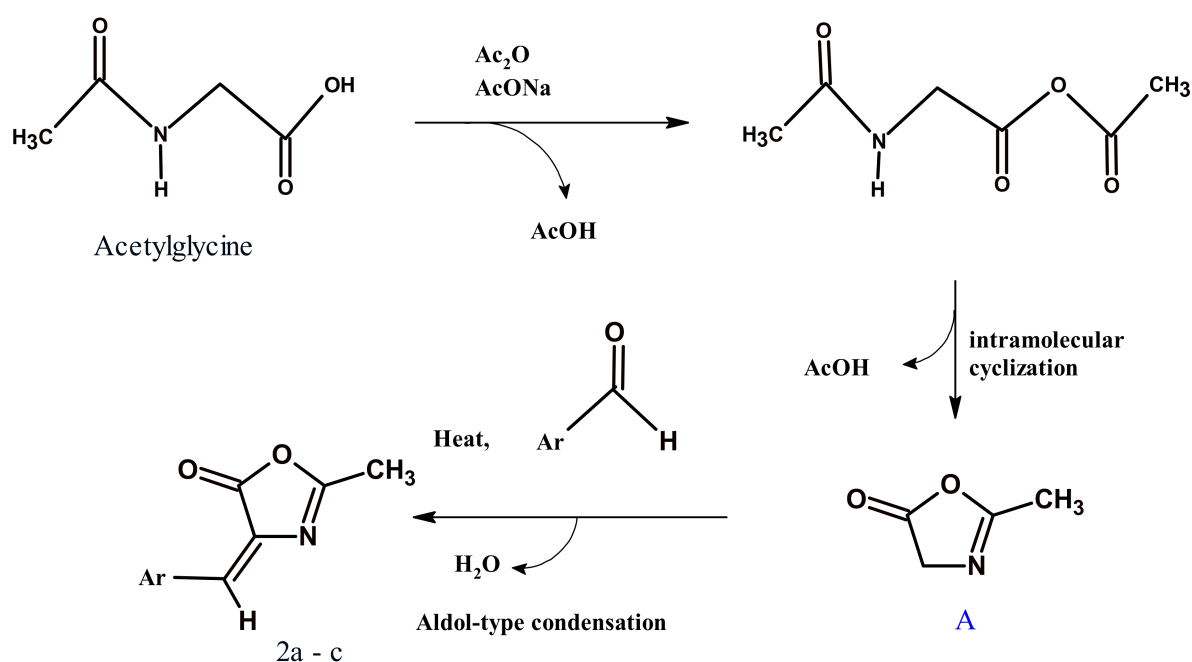
2.1. Chemistry

Here, we reported the synthesis of novel purine derivatives and the assessment of their antibacterial and antifungal activities. 5,6-Diaminouracils **1a-e**, the key starting material for the obtained compounds, were synthesized by the reaction between ethyl cyanoacetate and different urea derivatives followed by nitrosation and reduction by conventional methods [25,38,39]. The Erlenmeyer azlactones (**2a-c**), also known as 4-arylideno-5(4*H*)-1,3-oxazolones, were synthesized according to literature [40–43] through an aldol-type condensation of a glycine-based azlactone (A) with different aldehydes (Scheme 2).



Scheme 2. **2a:** Ar = C₆H₅, **2b:** 3-NO₂.C₆H₄, **2c:** 4-Cl.C₆H₄.

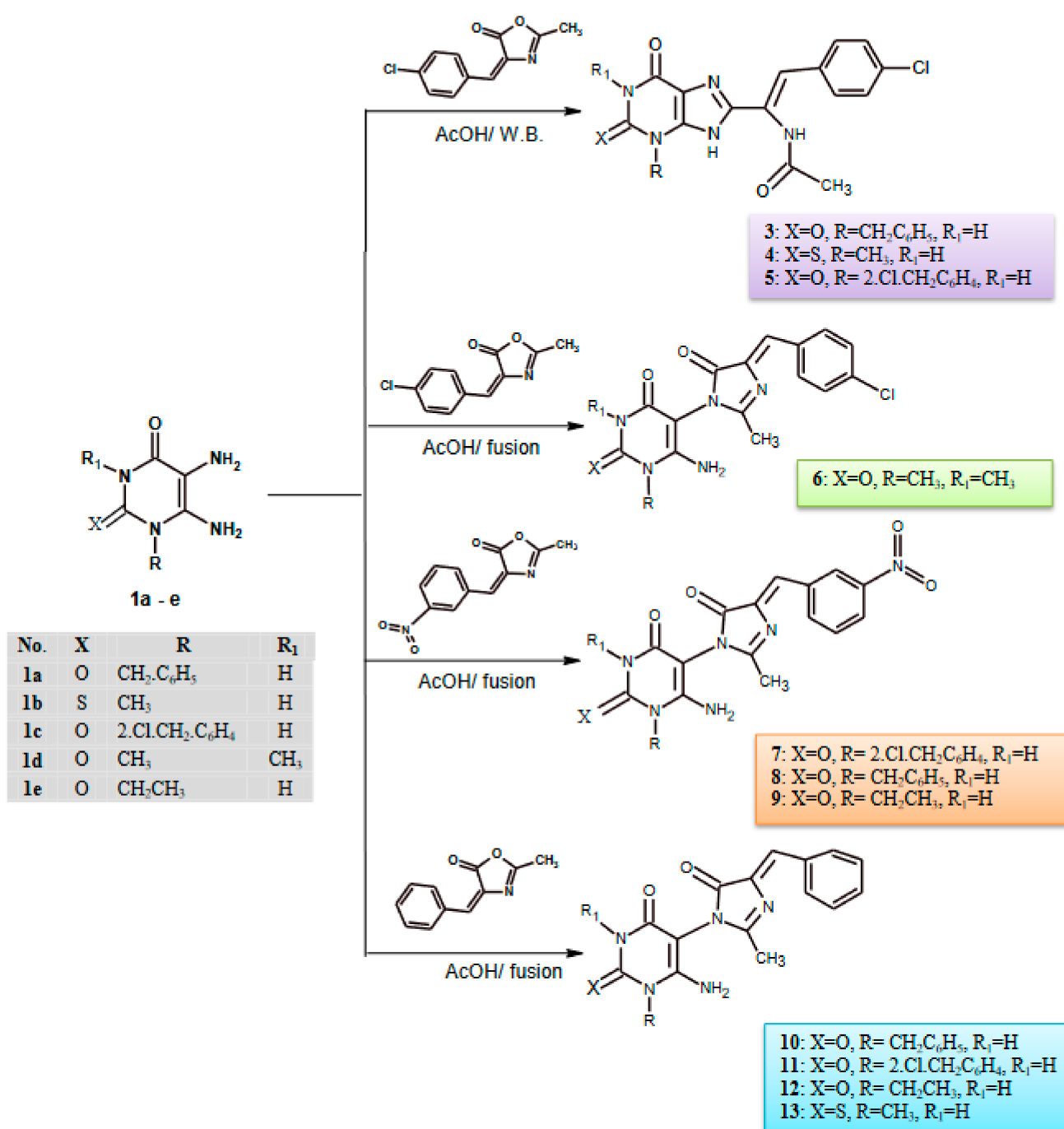
The mechanistic pathway for the formation of azlactones **2a-c** was explained in (Scheme 3).



Scheme 3. Mechanistic pathway for the synthesis of oxazolone derivatives **2a-c**.

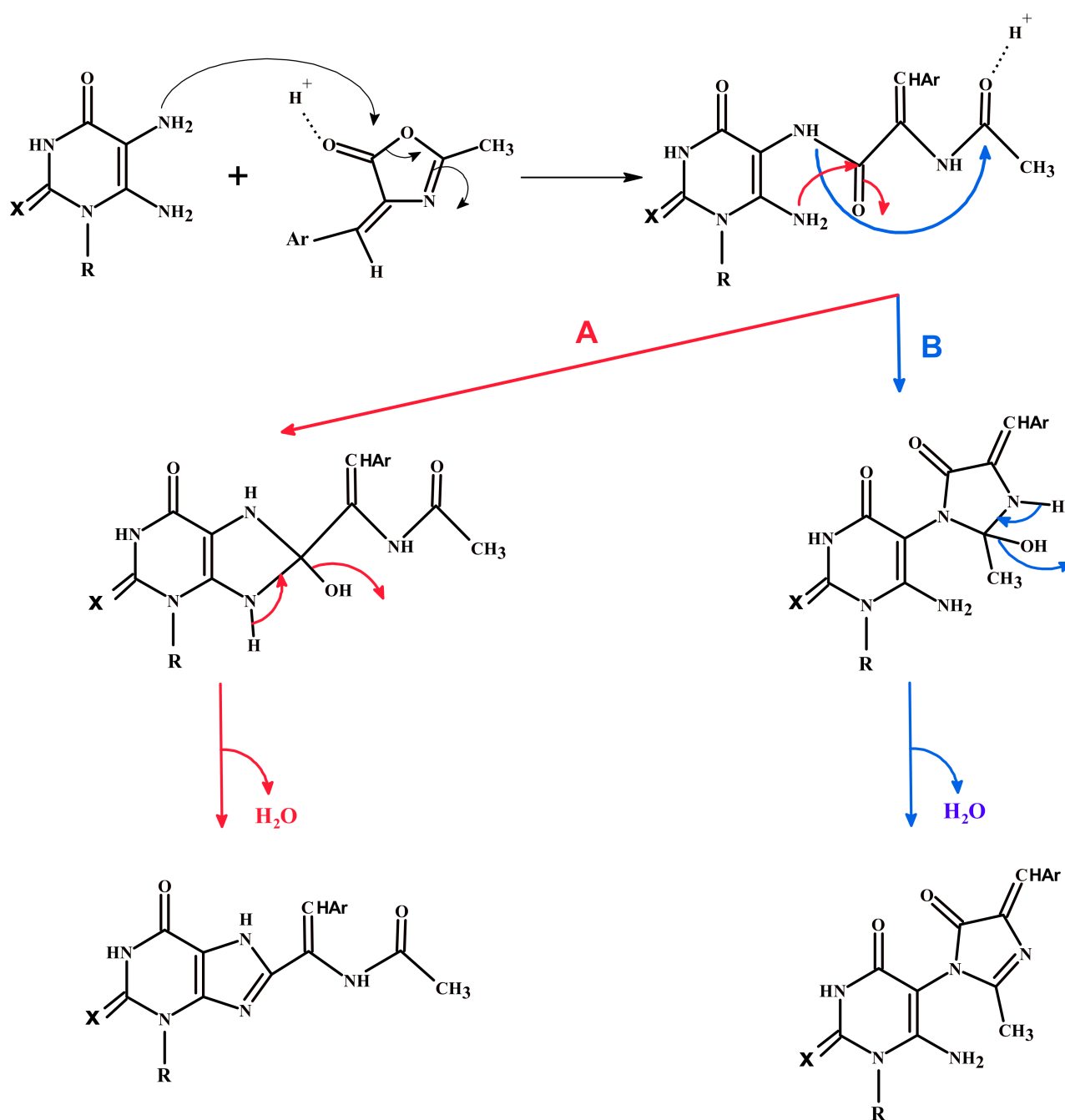
Moreover, N-Substituted-8-purinyl-2-substituted vinylacetamide **3-5** were prepared by heating 5,6-diaminouracils **1a-c** in water bath with azlactone **2c** in acetic acid for 1 h as illustrated in Scheme 4. The xanthine derivatives were crystallized from DMF/EtOH. Different analyses were applied to identify the resulting compounds. The most interesting observation in the $^1\text{H-NMR}$ spectra of compounds **3-5** showed the disappearance of both signals of NH_2 (5) and NH_2 (6) around δ 5.0–6.0 ppm in compounds **1a-c** and the appearance of signals of NH (7) around δ 12.74–12.66 ppm, NH signals of acetamide group around δ 9.48–9.46 ppm, a singlet signal of CH benzylidene around δ 6.98–6.56 ppm and the upfield singlet signals of methyl group of acetamide around δ 1.91–1.90 ppm. While the IR spectra of the compounds **3-5** displayed a stretching band of NH within the range ν 3294–3278 cm^{-1} and the C=O groups (Amide I), red-shifted within the range ν 1705–1620 cm^{-1} . $^{13}\text{C-NMR}$ spectra indicates the formation of compounds **3-5** through the appearance of the CH benzylidene around δ 112 ppm and the upfield signals of methyl group of acetamide around δ 23 ppm.

Analogously, 5,6-diaminouracils **1a-e** were heated under fusion with different 1,3-oxazolones in acetic acid affording 6-amino-1-substituted-5- arylimidazolyluracil **6-13** in a high yield (Scheme 4). Compounds **6-13** are characterized by the disappearance of the NH_2 (5) signals around δ 5.0–6.0 ppm, the presence of the NH_2 (6) signals around δ 7.41–7.23 ppm, in addition to the appearance of singlet signals of CH benzylidene around δ 7.15–6.95 ppm and the upfield singlet signals of methyl group at δ 2.22–2.09 ppm. The IR spectra of compounds **6-13** showed the stretching band of NH within the range ν 3347–3172 cm^{-1} and the C=O groups (Amide I) within the range ν 1735–1627 cm^{-1} , The strong asymmetric and symmetric NO_2 stretching bands of the nitro group were noted at ν 1519–1512 and 1388–1381 cm^{-1} . $^{13}\text{C-NMR}$ spectra prove the formation of compounds **6-13** through the appearance of the CH benzylidene around δ 124.38–121.08 ppm and the upfield signals of methyl group at the range δ 16.41–15.04 ppm.



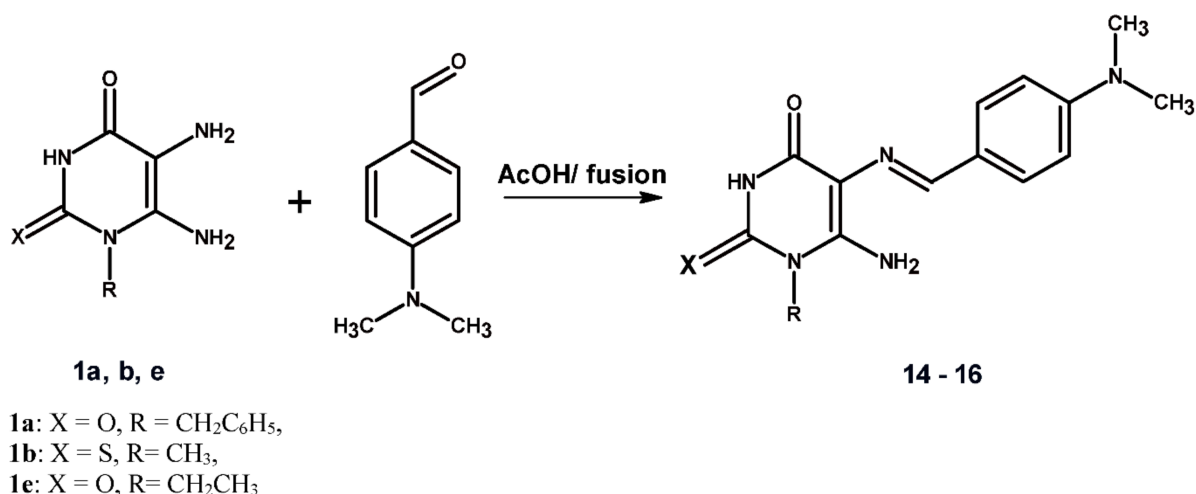
Scheme 4. The reaction of uracils with different azlactones 3-13.

Plausible mechanisms for these reactions are shown in Scheme 5 which takes place by two ways **A** or **B**. The acidic medium **A** first activates oxazolone carbonyl group via protonation which indicated by the blue arrows. Then, oxazolone ring is ruptured due to uracil amino group (5) attack. After that, pyrimidoimidazolone derivatives are obtained in the procedure of intramolecular cyclization **B**. Otherwise the amino group (6) attack the carbon of carbonyl group of oxazolone via protonation, then imidazolopyrimidine-2,4-diones were formed.



Scheme 5. The suggested mechanism for the synthesis of xanthine and imidazolone derivatives.

Treatment of compounds **1a,b,e** with 4-dimethylaminobenzaldehyde in acetic acid was heated under fusion for 5–7 min to yield the target Schiff base derivatives **14–16** in high yields (Scheme 6). The compound **14** was synthesized by heating 5,6-diamino-1-methyl-2-thiouracil (**1b**) with 4-dimethylaminobenzaldehyde in dioxan at 80 °C with stirring for 2 h, as described by Nagamatsu [44]. Our improved method for synthesis of compound **14** has been conducted at 5–7 min, with 96% yield and affordable lower cost.



Scheme 6. Formation of Schiff base.

The structures of the synthesized Schiff base derivatives were confirmed on the basis of their IR, ¹H-NMR, ¹³C-NMR, mass spectral data and elemental analysis.

2.2. Biological Activity

2.2.1. Antimicrobial Activity

The antimicrobial efficacy of the synthesized uracil derivatives was evaluated by disc diffusion assay for the antibiotic resistant bacteria; *E. coli*, *Pseudomonas* sp., *Salmonella* sp., *Staphylococcus aureus* and *Bacillus* sp., in addition to pathogenic fungi (*A. flavus* and *C. albicans*). After desired incubation, the biological activity of the tested compounds was evaluated from the diameter of the inhibition zones. From the diameter of inhibition zones (Table 1), compounds 3 and 6 displayed the highest antifungal activity towards *C. albicans* (10 mm), *A. flavus* (2 mm), as well as antibacterial activity towards Gram positive bacteria *S. aureus* (1.0 mm) and Gram negative bacteria *E. coli* (4 mm). Practically, the compounds 3 and 6 exhibited the same physiological effect on the growth of bacteria and fungi revealing their chemical proximity. The compound 16 displayed the highest antifungal activity; *A. flavus* (10 mm) and *C. albicans* (12 mm), as well as highest activity against *E. coli* (7 mm), *Pseudomonas* sp. (1.9 mm) and *Bacillus* sp. (1.2 mm). The antibacterial and antifungal activities of the tested compounds were normalized to the authentic commercial antifungal (Fluconazole) and antibacterial (Bacimethrin, Primisol) drugs. As well as, the compounds # 11, 12 and 13 exhibited a strong antifungal activity against *C. albicans*, *A. flavus* and *E. coli*. However, the compounds 4, 5, 7, 8, 10, displayed a mild activity towards the tested microorganisms. Obviously, a fluctuation has been observed on the activity of the synthesized compounds towards the tested microorganisms, suggesting the structure-activity relationships of the synthesized compounds for each microorganism. DMSO at the 10% has been used as negative control, displaying no signs of antimicrobial activity towards the tested microorganisms.

For further authentication of the antimicrobial activity of the tested compounds, different concentration of each compound was used, and after the desired incubation the kinetics of microbial growth of each microorganism was determined (Figure 1). The IC₅₀ values for each compound against the tested microorganisms were summarized in Table 2. The compounds 3, 6, 12, and 13 exhibited the highest activity against *E. coli* as revealed from the IC₅₀ values that was 1.8–1.9 µg/mL. From the IC₅₀ values, the compound 16 displayed a significant activity towards *C. albicans* (0.82 µg/mL), *A. flavus* (1.2 µg/mL), *E. coli* (1.9 µg/mL), *Salmonella* sp. (1.5 µg/mL), *Pseudomonas* sp. (2.1 µg/mL), *S. aureus* (2.6 µg/mL) and *Bacillus* sp. (2.1 µg/mL).

Table 1. Antimicrobial activity of the synthesized derivatives of 3-16 towards *C. albicans*, *A. flavus*, *E. coli*, *S. aureus*, *Pseudomonas sp.*, and *Salmonella sp.*

Cpd	Diameter of Inhibition Zone (mm)						
	Fungi		Gram Negative Bacteria			Gram Positive Bacteria	
	<i>C. albicans</i>	<i>A. flavus</i>	<i>E. coli</i>	<i>Salmonella sp.</i>	<i>Pseudomonas sp.</i>	<i>S. aureus</i>	<i>Bacillus sp.</i>
10% DMSO	-	-	-	-	-	-	-
3	10 ± 0.8	2	4 ± 0.2	0.2 ± 0.01	0	2 ± 0.01	0.7 ± 0.01
4	2	0	2	0.1	0	1 ± 0.01	0.1
5	2	0	2	0	0	0.8 ± 0.01	0.8 ± 0.04
6	10 ± 0.6	2	4 ± 0.1	0	0	1 ± 0.01	0.9 ± 0.01
7	2	0	2	0	0	0	0
8	2	3	2	0	1.8 ± 0.01	0.2	0
9	5 ± 0.2	2	3 ± 0.3	0	0.9 ± 0.05	0	0.8 ± 0.03
10	4 ± 0.2	0	4 ± 0.23	0	0	0	0
11	6 ± 0.3	3	3 ± 0.3	0	0	0	0
12	8 ± 0.4	4	5 ± 0.22	0	1.5 ± 0.01	0.3	0
13	6 ± 0.2	3	4 ± 0.23	0	0	0.4	0.9 ± 0.01
14	2	2	2	0	1.9 ± 0.03	0	0
15	7 ± 0.5	3	3 ± 0.1	0.1 ± 0.01	1.8 ± 0.03	0	0.8 ± 0.03
16	12 ± 0.3	10	7 ± 0.2	0.2 ± 0.01	1.9 ± 0.04	0.7	1.2 ± 0.04
Fluconazole	2.1 ± 0.1	2.9 ± 0.1	0	0	0	0	0
Bacimethrin			0.9 ± 0.2	0.6 ± 0.2	0.8 ± 0.2	0.9 ± 0.2	0.7 ± 0.2
Primsol			0.6 ± 0.09	0.5 ± 0.02	0.4 ± 0.02	0.3 ± 0.01	0.4 ± 0.3

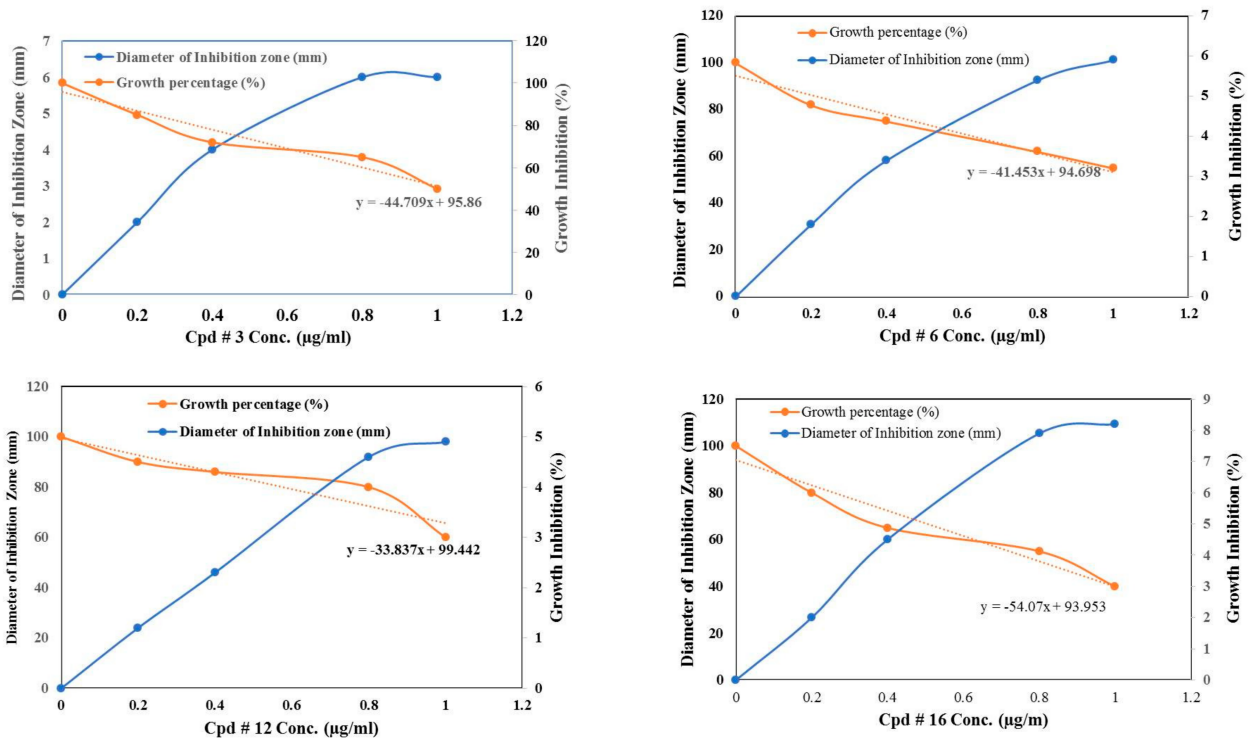


Figure 1. Kinetics of inhibition of the compounds 3, 6, 12 and 16 on *C. albicans*.

Table 2. IC₅₀ values of the tested compounds against the various multidrug resistance microorganisms.

IC ₅₀ Values of the Synthesized Compounds								
Cpd	Fungi		Gram Negative Bacteria			Gram Positive Bacteria		
	<i>C. albicans</i>	<i>A. flavus</i>	<i>E. coli</i>	<i>Salmonella</i> sp.	<i>Pseudomonas</i> sp.	<i>S. aureus</i>	<i>Bacillus</i> sp.	
3	1.07	4.9	1.8	3.9	5.2	2.8	2.4	
4	5.0	6.0	4.8	2.1	5.7	2.1	3.2	
5	6.0	7.5	4.5	5.0	6.1	2.9	2.8	
6	1.02	4.2	1.9	4.9	5.1	2.9	2.2	
7	5.3	8.0	5.1	6.2	7.1	5.2	5.2	
8	5.1	7.5	4.9	7.9	1.9	5.4	5.5	
9	4.9	3.8	4.1	8.0	4.2	6.0	3.8	
10	4.2	8.0	2.1	7.9	2.9	6.2	4.9	
11	3.2	3.2	2.2	7.0	3.9	6.3	5.5	
12	1.46	2.9	2.11	7.2	2.2	3.1	6.9	
13	3.3	3.9	1.9	2.3	6.9	3.2	2.8	
14	4.2	3.9	5.1	8.1	2.8	4.0	4.9	
15	4.1	4.2	4.9	7.2	2.9	5.1	5.3	
16	0.82	1.2	1.98	1.5	2.1	2.67	2.1	
Fluconazole	0.6 ± 0.1	6.0 ± 0.1	0	0	0	0	0	
Bacimethrin	0	0	3.9 ± 0.6	4.8 ± 0.1	5.1 ± 0.1	4.2 ± 0.1	3.9 ± 0.1	
Primsol	0	0	4.3 ± 0.4	4.8 ± 0.1	4.6 ± 0.1	5.0 ± 0.1	4.3 ± 0.1	

2.2.2. TEM Analysis of Microorganisms in Response to the Tested Compounds

The cytomorphological deformations of the microorganisms in response to the tested compounds were evaluated by TEM. The effects of the most potent uracil derivative-compounds on the cellular structure of Gram positive and Gram-negative bacteria were assessed. The influence of the most potent compounds on the cellular structures of *E. coli* was assessed (Figure 2). An obvious cellular deformation on the cell wall and cell membrane was observed upon treatment with the compounds **3**, **12**, **13**, **14** and **16**. With treatment of *E. coli* by the compounds at their MIC values, a complete distortion and ruptures to the bacilli type, comparing to regular bacillus shape of control. The cellular structure of *Pseudomonas* sp., upon treatment with the compounds **3**, **12**, **13**, **14**, and **16** was evaluated by TEM. From the results of TEM analysis (Figure 3), a complete morphological deformation to bacterial cells from short rod cells into rounded cells, was observed. A complete rupture on the cell walls and cell membranes was observed, with obvious leakage to the cellular organelles, caused by the partial ruptures on the cell walls. The rationality of destructive effect of the compound **16** may be due to the suppression of pivotal biological secondary metabolites especially the proper cellular morphogenesis as revealed from the binding affinity with ACP domain of polyketide synthase type I. The cellular deformation of the *Klebsiella* sp., in response to the compounds **3**, **12**, **13**, **14** and **16** has been observed (Figure 4), a complete distortion to the cellular identity of *Klebsiella* in response to treatment with these compounds. From the TEM micrograph, a dramatic deformation has been noticed to the bacterial cell walls and various organelles in response to the tested compounds. A remarkable alternations and deformation to the cells, irregularity on shape, loss of symmetry, equivocal distribution of the cytoplasmic organelles, especially the cell wall and plasma membrane that becoming a highly denser, have been observed. The powerful antibacterial activity of the compounds **12** and **16** elaborates from their higher binding affinity with the ACP domains of PKS type I [45] and DNA gyrase [46], blocking the synthesis of essential secondary metabolites and DNA replication. Increase on the plasma membrane permeability causes a strong cracking to the bacterial cell leading to a visual release of the cytoplasmic materials. With the treatment, almost all cellular organelles were strongly deforming, in contrary to the control cells which are usually short bacilli, with a multilayered cell surface consisting of an outer membrane, a peptidoglycan layer in the periplasmic space, the cytoplasmic membrane was relatively uniform [47].

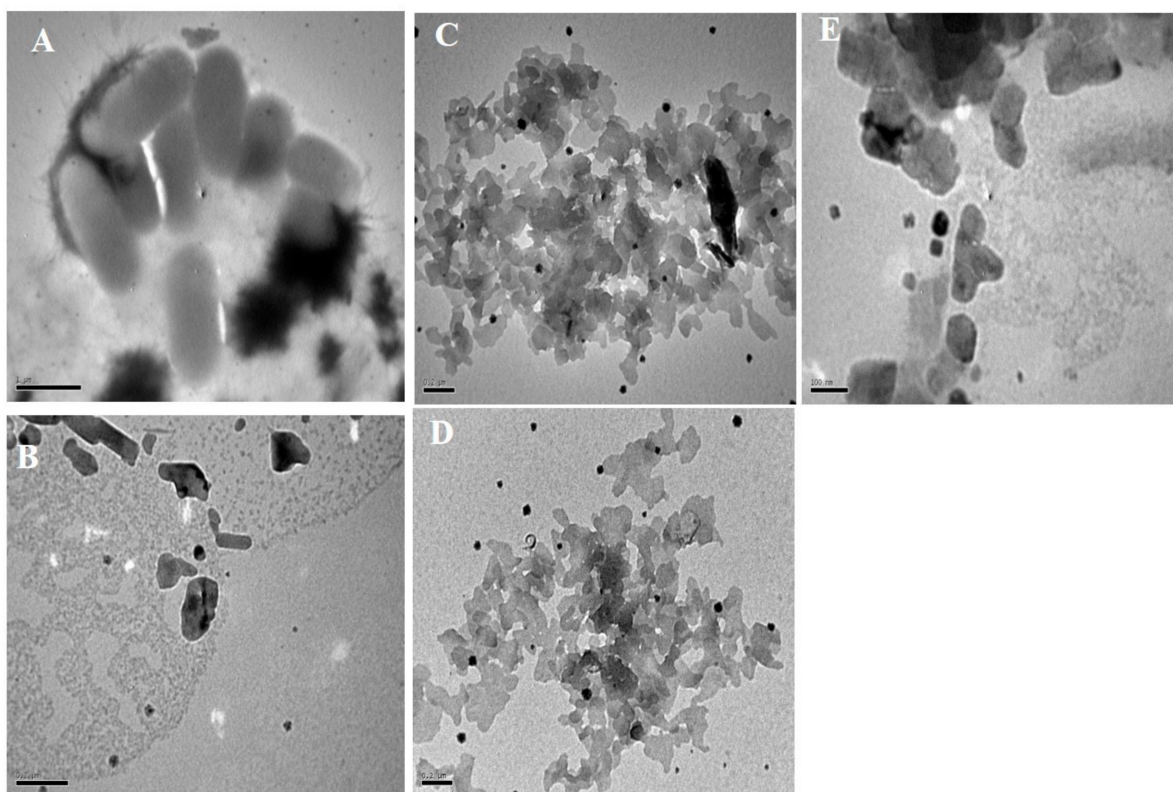


Figure 2. Effect of the tested compounds 3, 12, 13 and 16 on structural identity of *E. coli*. TEM Microgram of *E. coli* (Control, (A)) and presence of compounds 3 (B), compound 12 (C), compound 13 (D) and compound 16 (E).

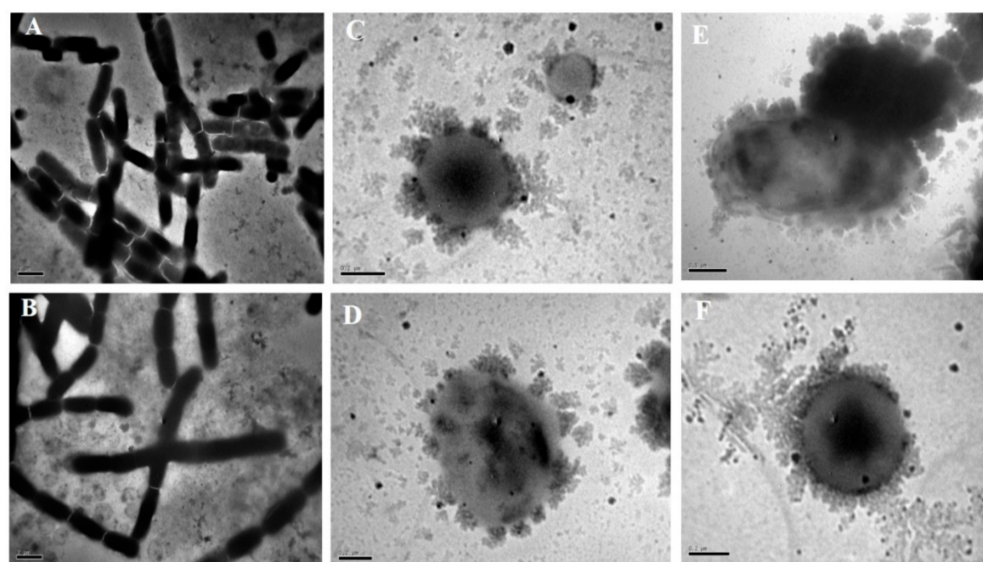


Figure 3. Effect of the tested compounds 3, 12, 13, 14 and 16 on structural identity of *Pseudomonas* sp. TEM Microgram of *Pseudomonas* sp. (Control, (A)) and presence of compounds 3 (B), compound 12 (C), compound 13 (D) and compound 14 (E) and compound 16 (F).

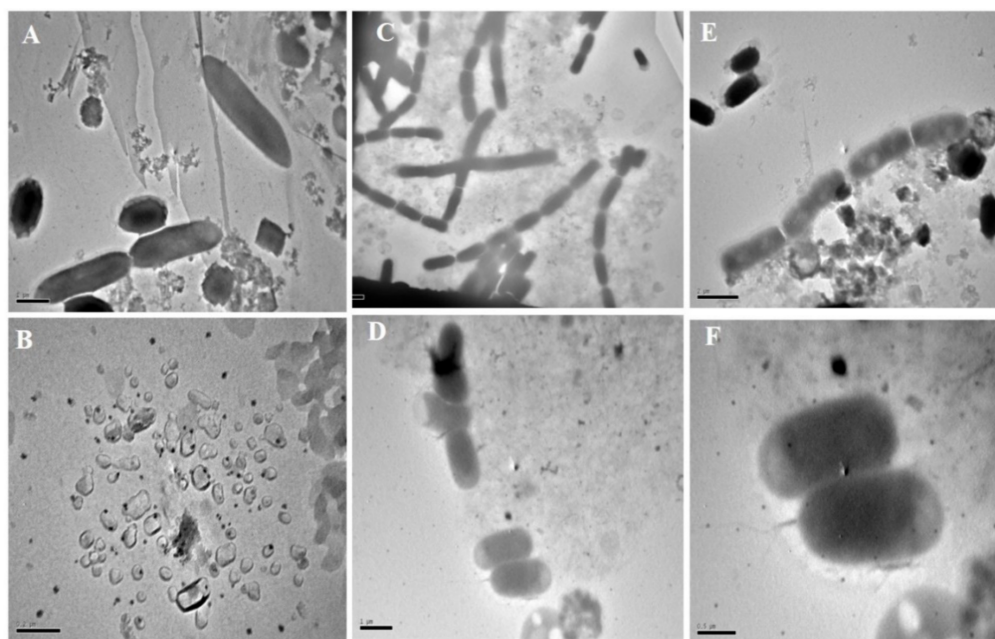


Figure 4. Effect of the tested compounds **3**, **12**, **13**, **14** and **16** on structural identity of *Klebsiella* sp. TEM Microgram of *Klebsiella* sp. (Control, (A)) and presence of compounds **3** (B), compound 12 (C), compound 13 (D) and compound 14 (E) and compound 16 (F).

2.2.3. Cytotoxicity Analysis

Cytotoxicity Assay

The cytotoxicity of the experimental compounds was evaluated towards VERO-E6 cells using the (MTT) assay. As revealed from the half maximal cytotoxic concentration (CC_{50}), the tested compounds **3**, S-Aza **1**, **5**, **6**, **8**, **11**, **12**, **13**, **14**, **9** displayed relatively no signs of toxicity in which the CC_{50} values were ranged from 160 to 676 $\mu\text{g}/\text{mL}$ as shown from the Supplementary Material (Figure S4). Negative control of 10% DMSO has been used. The DMSO (10%) did not display any signs of toxicity to the VERO-E6 cells.

2.3. Molecular Docking Study

To take one step further, and to determine the mode of action of the tested compounds as potential anti-microbial agents, molecular-docking study was employed to determine the binding modes against three important proteins implicated in fungal and bacterial targeting mechanism including APC, DNAG and PBP. These targets were selected based on structure activity relationship with the corresponding co-crystallized ligands with our tested compounds. The cocrystal ligand for the three proteins (PNS for APC protein, CBN for DNAG protein, and PNM for PBB protein) were redocked to assure the validity of the docking parameters and methods to represent the position and orientation of the ligand detected in the crystal structure. The difference of RMSD value between cocrystal ligands to the original cocrystal ligand was $<2 \text{ \AA}$ which approved the accuracy of the docking protocols and parameters.

To elucidate the mode of action of the most promising antimicrobial compounds “**3**, **12**, **13** and **16**” docking studies were conducted. Compounds **3**, **12**, **13** showed an affinity to bind with APC protein active site, that was evidenced by low binding energy compared to reference ligand 4'-Phosphopantetheine (PNS) (-5.1 , -5.1 , -5.2 Kcal/mol , respectively), while compound **16** has the same binding free energy value of the reference ligand (-4.5 Kcal/mol) (Table 3). All tested compounds formed one hydrogen bond with key amino acid residue Glu65 (Table 3). Docking results against DNAG protein, showed less binding affinity of all tested compounds against this protein, which was evident by high free of energy for all compounds compared to reference ligand Clorobocin (CBN) (Table 3). In addition, docking score against PBP protein, showed

a favorable binding affinity to this protein, as revealed from the low values of energy of free binding compared to reference ligand penicillin G (PNG) (Table 3). Compounds 3, and 12 showed the lowest values binding free energy (−8.7 and −8.2 Kcal/mol), compared to PNG (−6.7 Kcal/mol), moreover compound 3 formed one hydrogen bond interaction with amino acid (ASN674: 2.006 Å), while compound 12 formed three hydrogen bonds with the key amino acid residues in the PBP pocket (SER470: 2.118; SER434: 3.269; THR672: 2.797) (Table 3), and (Figures 5 and 6).

Table 3. Results of the docking study of compounds against fungal type I polyketide synthase (ACP), DNA gyrase, and Baumannii penicillin-binding protein (PBP) in comparison to the corresponding co-crystallized ligands.

APC Protein (PDB: 2KR5)				
Compounds	Free Binding of Energy (Kcal/mol)	H-Bond		
		No of H-Bond	Amino Acid Residues	Length Å
3	−5.1	1	GLU65	2.261
12	−5.1	1	GLU65	2.348
13	−5.2	1	GLU65	2.358
16	−4.5	1	GLU65	1.984
PNS	−4.5	2	GLU65	2.265
			ASP71	2.559
DNAg Protein (PDB: 1KZN)				
Compounds	Free Binding of Energy (Kcal/mol)	H-Bond		
		No of H-Bond	Amino Acid Residues	Length Å
3	−8.2	1	THR165	3.074
12	−7.2	2	ASP49	2.576
			ASN46	3.395
13	−7.4	2	ASP49	2.573
			ASN46	3.368
16	−7.1	2	ASP73	2.276
			ASN46	2.392
CBN	−9.3	4	ASN46	3.142
			ARG136	2.930
			ARG136	2.923
			ARG136	3.244
PBP Protein (PDB: 3UDI)				
Compounds	Free Binding of Energy (Kcal/mol)	H-Bond		
		No of H-Bond	Amino Acid Residues	Length Å
3	−8.7	1	ASN674	2.006
12	−8.2	2	SER470	2.118
			THR672	2.797
13	−7.6	2	SER470	2.458
			THR672	3.040
16	−7.3	3	SER470	2.697
			SER487	3.278
			THR672	2.916
			TYR670	3.006
			TYR670	3.035
PNS	−7.2	5	SER434	3.078
			THR672	3.128
			THR672	2.310

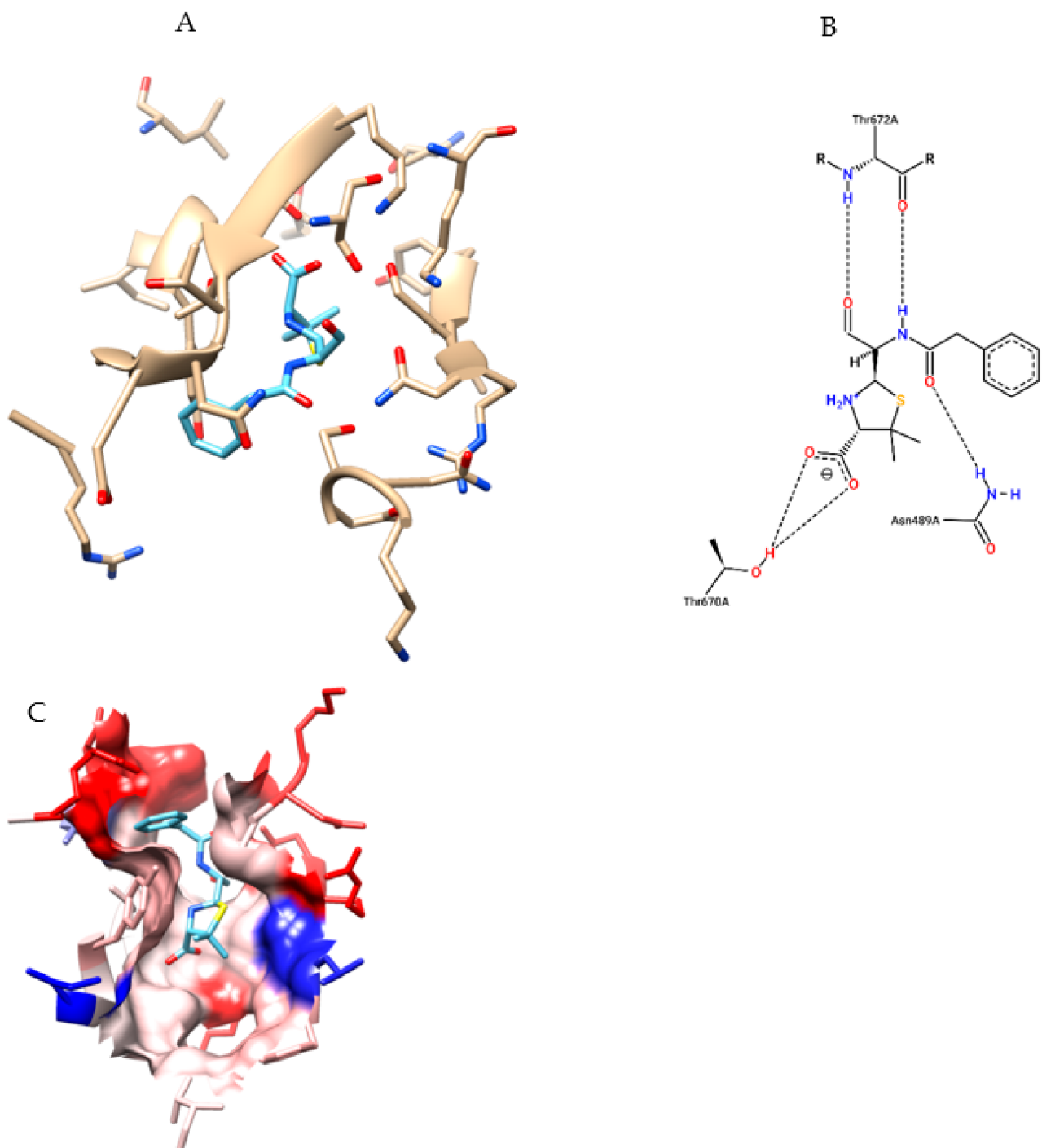


Figure 5. Reference ligand interaction with PBP protein, (A) 3D interaction, (B) hydrogen bond formation, (C) Hydrophobic interaction (represented by blue color).

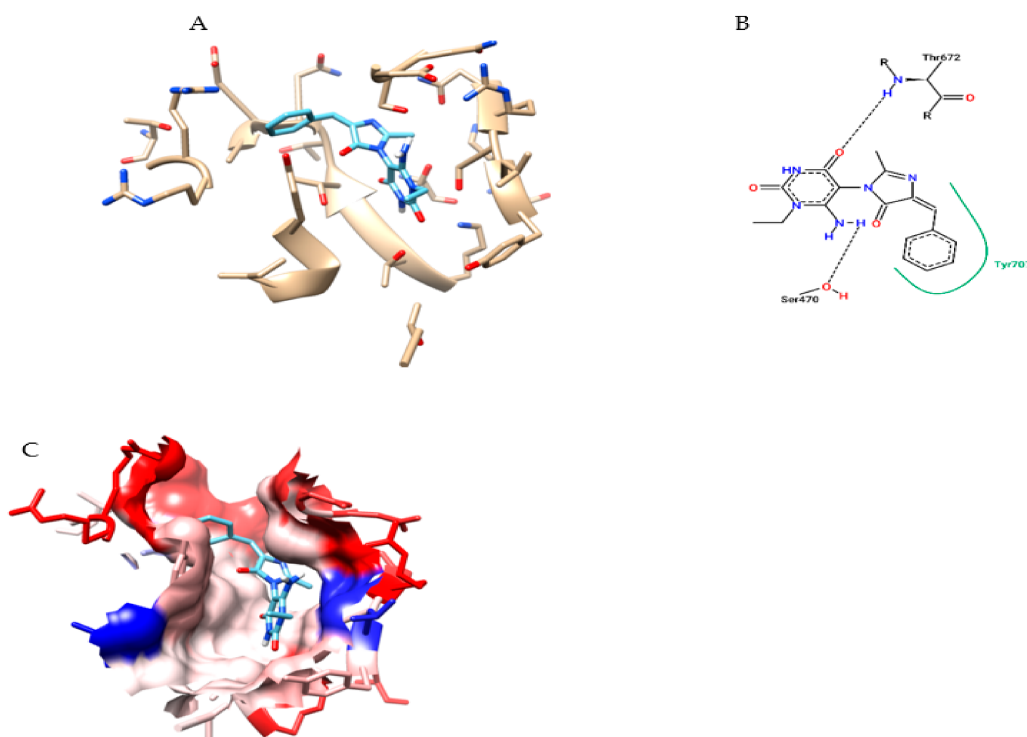


Figure 6. Compound **12** interaction with PBP protein, (A) 3D interaction, (B) hydrogen bond formation, (C) Hydrophobic interaction (represented by blue color).

2.4. Pharmacokinetics and ADME Activity

To predict the physicochemical and drug-likeness properties, bioinformatics study for the compound **12** was carried out (Table 4). Bioavailability Radar has been generated to check the suitable physicochemical properties for oral bioavailability, based on 6 characters including (lipophilicity: XLOGP3 between -0.7 and $+5.0$, size: M_W between 150 and 500 g/mol, polarity: TPSA between 20 and 130 Å, solubility: log S not higher than 6, saturation: fraction of carbons in the sp^3 hybridization not less than 0.25, and flexibility: no more than 9 rotatable bonds) (Table 4, Figure 7). Compound **12** exhibited good bioavailability, and good water solubility, while it showed good pharmacokinetics with high gastrointestinal absorption (GI), and it does not permit blood brain barrier (BBB) as it depicted in the boiled Egg model (Figure 8). In addition, compound **12** has good drug likeness properties according to Lipinski rule of five for drug discovery without any violation.

Table 4. Physicochemical properties and drug-likeness.

Properties	Compound 12
Formula	$C_{17}H_{17}N_5O_3$
Molecular weight	339.35
Num. of heavy atoms	25
Num. of aromatic heavy atoms	12
Num. of rotatable bonds	3
Num. H-bond donors (HBD)	2
Num. H-bond acceptor (HBA)	4
Molar reactivity	103.26
Topological Polar Surface area (TPSA)	113.55
Lipophilicity (Log P)	2.04
Water solubility (Log S)	-2.39

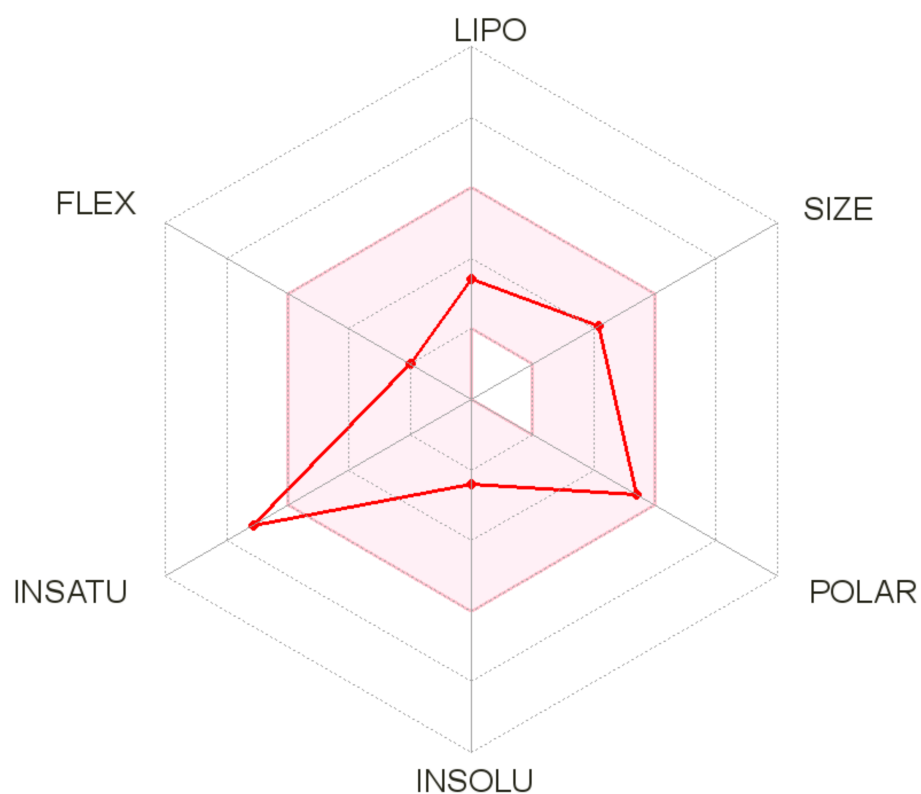


Figure 7. The Bioavailability Radar shows that compound **12**, represented by central red lines fits in the pink area which is the optimal range for each property.

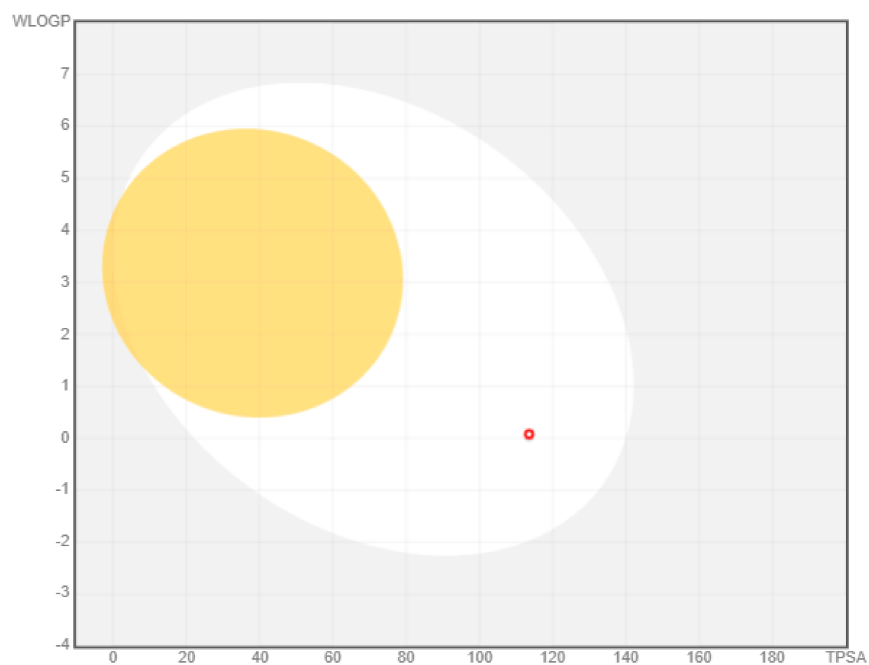


Figure 8. Pharmacokinetics bioled egg model. Yellow colour represents blood brain barrier (BBB), while colour represents gastrointestinal absorption for the selected drugs. Red circle represents compound **12**.

2.5. Computational Details

2.5.1. Structural Parameters and Models

N-(1-(3-benzyl-2,6-dioxo-2,3,6,7-tetrahydro-1H-purin-8-yl)-2-(4-chlorophenyl)vinyl)acetamide, compound **3**. The activity of hetero cyclic compounds is mainly determined by its structure, this compound has many characteristic structural features. The bond length N22-C21 is 1.395 Å, C21-N0 is 1.389 Å, there is a single bond characters C and N atoms [48], the bond lengths of N17-C10 and N11-C10 are 1.269 and 1.339 Å, respectively, whereas the N17-C10 bond has double bond characters, while the N11-C10 has single bond characters [48]. Detailed analysis of corresponding bond lengths in various hetero cyclic compounds were given elsewhere [49]. All distances and angles between the atoms of the ligand I was given in (Table 5). The C21-O24 bond length is 1.208 Å, while the C19-O23 bond length is 1.210 Å [50], C13- N12 is 1.384 Å [49] and the C13=O14 bond length of carbonyl group is 1.209 Å [50].

Table 5. Equilibrium geometric parameters bond lengths (Å), bond angles (°), dihedral angles (°), total energy (k cal/mol), heat of formation (k cal/mol), Mulliken charges over atoms and dipole moment of the N-(1-(3-benzyl-2,6-dioxo-2,3,6,7-tetrahydro-1H-purin-8-yl)-2-(4-chlorophenyl) vinyl)acetamide, compound **3** by using DFT calculations.

Bond Length (Å)					
C1-C2	1.346	C13-N12	1.384	N20-C21	1.389
C2-C3	1.345	C13-O14	1.209	C21-N22	1.395
C3-C4	1.348	C13-C15	1.521	C21-O24	1.208
C4-C6	1.354	C10-N11	1.339	C18-N22	1.351
C5-C6	1.343	N11-C16	1.334	N22-C25	1.453
C1-C5	1.341	C16-C18	1.338	C25-C26	1.556
C1-C17	1.726	N17-C18	1.348	C26-C27	1.346
C4-C8	1.351	C10-N17	1.269	C27-C28	1.342
C8-C9	1.353	C16-C19	1.349	C28-C29	1.341
C9-C10	1.346	C19-N20	1.377	C29-C31	1.342
C9-N12	1.354	C19-O23	1.210	C30-C31	1.342
				C26-C30	1.346
Bond Angle (°)					
C3C4C8	124.63	C9N12C13	124.18	C9C10N11	123.47
C6C4C8	118.83	N12C13C15	122.51	C18N22C25	120.23
C4C8C9	131.89	N12C13O14	118.39	C25N22C21	120.71
C8C9N12	113.55	O14C13C15	119.04	C26C25N22	113.98
C8C9C10	126.94	C9C10N17	125.31	C25C26C27	119.35
				C25C26C30	122.79
Dihedral Angles (°)					
C3C4C8C9	18.74	C10C9N12C13	82.58	C26C25N22C18	-84.71
C6C4C8C9	-165.54	C9N12C13C15	-19.77	C26C25N22C21	87.88
C4C8C9N12	-179.95	N12C9C10N11	23.75	N22C25C26C20	-4.19
C4C8C9C10	20.23	N12C9C10N17	-154.23	N22C25C26C27	175.85
C8C9N12C13	-105.95	C10N17C18N22	178.05	C8C9N10N17	102.31
O23C19N20C21	178.85	O24C21N20C19	179.53		
Mulliken charges					
C1	0.237	C10	0.217	C21	0.501
C17	-0.295	N11	-0.107	N20	-0.324
N12	-0.284	N17	-0.334	O24	-0.432
C13	0.424	C16	-0.111	C19	0.425
C9	0.114	C18	0.246	O23	-0.446
O14	-0.488	N22	-0.198		
Total energy/k cal/mol				-172,059.722	
Heat of formation k cal/mol				-10,607.049	
Total dipole moment/D				3.078	

The molecule is a highly sterically-hindered, there are three aromatic rings. The molecule is non-planar, there are two planes one occupied by the two aromatic rings and other plane occupied by the purine ring and also, the two planes are perpendicular respect to each other. The purine ring is lying out of plane of the plane occupied by the two aromatic rings, the dihedral angles C26C25N22C18 is $-84.71^\circ \approx 90^\circ$ and the acetamide group is lying in perpendicular plane respect to purine ring system, the C10C9N12C13 is $82.58^\circ \approx 90^\circ$, where the values are neither zero nor 180° . The C10N17C18N22, $178.05^\circ \approx 180^\circ$, also the dihedral angles: N22C25C26C27, $-175.85^\circ \approx 180^\circ$ and N22C25C26C20, $-4.19^\circ \approx 0.00^\circ$, where the values are nearly zero or 180° . Figure 9, the terminal benzyl group is lying in perpendicular plane respect to purine ring system, with a dihedral bond angle C8C9N10N17 is $102.31^\circ \approx 90^\circ$, Figure 9 shows the optimized geometrical structure of the compound (3), N-(1-(3-benzyl-2,6-dioxo-2,3,6,7-tetrahydro-1H-purin-8-yl)-2-(4-chlorophenyl)vinyl)acetamide, the dihedral angles O23C19N20C21 is $178.85^\circ \approx 180^\circ$ and O24C21N20C19 is $-179.53^\circ \approx 180^\circ$, which confirms that the O23 and O24 are lying in the same plane of the nitrogen atom N20 of purine ring. The oxygen atom O14 of acetamide group is lying in trans position respect to the C9 which bonded with purine ring with dihedral angle $168.98^\circ \approx 180^\circ$, while the others two oxygen atoms O23 and O24 are lying in the same plane away from the plane occupied by O14 of acetamide group, this confirms that one oxygen atoms of these three atoms can be chelated as donor with any acceptor according to the value of accumulated charge density lying on it. The value of bond angle C4C8C9 is 131.89° , C26C25N22 is 113.98° , C8C9C10 is 126.94° and C9N12C13 is 124.18° reflects on sp² hybridization on the C8, C25, C9 and N12.

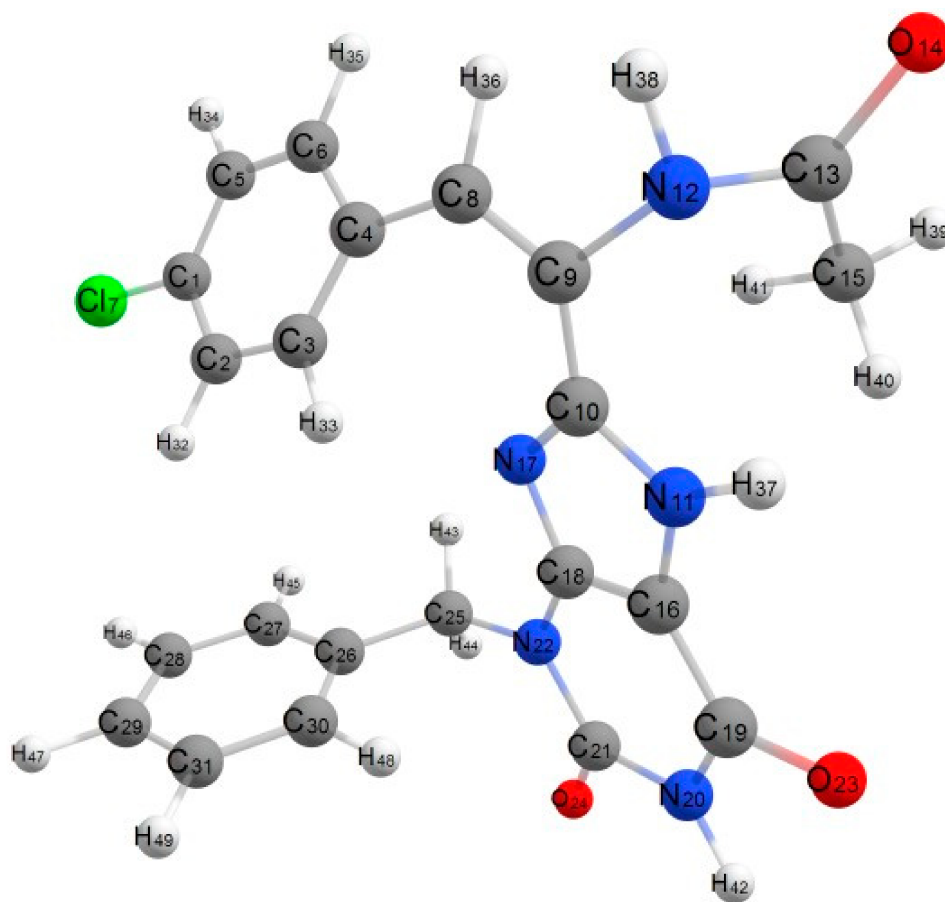


Figure 9. Optimized geometrical structure of compound (3), N-(1-(3-benzyl-2,6-dioxo-2,3,6,7-tetrahydro-1H-purin-8-yl)-2-(4-chlorophenyl)vinyl)acetamide by using DFT calculations.

There is building up of charge density on the hetero atoms, nitrogen and oxygen atoms, the highest charged atoms are O14 of carbonyl group in acetamide with -0.488 ,

while the others two oxygen atoms O23 and O24 have lower charge density values, -0.446 and -0.432 , so the active site in this compound is O14 as set in docking study in biological investigation, the compound **3** favors bonding with any receptor through the oxygen atom O14 of carbonyl group. The accumulated charge density on nitrogen atoms N11, N17, N20, N22 and N12 involved in this compound are -0.107 , -0.334 , -0.432 , -0.198 and -0.284 , respectively. The value of energy of this compound is $-172,059.722$ kcal/mol, heat of formation of this compound is $-10,607.049$ kcal/mol and slightly weak dipole $3.078D$. Detailed analysis of corresponding bond lengths in various hetero cyclic compounds were given elsewhere [51,52]. All distances and angles between the atoms of the ligand are given in (Table 5).

6-Amino-5-(4-benzylidene-2-methyl-5-oxo-4,5-dihydro-1H-imidazol-1-yl)-1-ethylpyrimidine-2,4(1H,3H)-dione, compound **12**

The bond length C5-N4 is 1.381\AA , C5-N6 is 1.388\AA and the N13-C17 bond length is 1.368\AA , so there is a single bond characters C and N atoms [48], the bond lengths of N16-C17 is 1.352\AA , whereas this bond has a double bond characters [48]. Detailed analysis of corresponding bond lengths in various hetero cyclic compounds were given elsewhere [49]. All bond distances and angles between the atoms of the compound **12**, 6-amino-5-(4-benzylidene-2-methyl-5-oxo-4,5-dihydro-1H-imidazol-1-yl)-1-ethylpyrimidine-2,4(1H,3H)-dione are given in (Table S1). The C3-O7 and C5-O8 bond lengths of the pyrimidine ring are 1.211\AA and 1.208\AA [50], while the C14-O18 of the imidazole ring is 1.209\AA .

The pyrimidine ring is lying out of plane of the plane occupied by the others two aromatic rings, the dihedral angles C17N13C1C3 and C17N13C1C2 are $109.33^\circ \approx 90^\circ$ and $-70.47^\circ \approx 90^\circ$, respectively, where the values are neither zero nor 180° . These values confirm that the pyrimidine ring is lying in perpendicular plane respect to the central aromatic imidazole ring of the compound. Also, the value of dihedral angle of C5N6C9C11 is $90.54^\circ \approx 90^\circ$, this value confirms that the terminal ethyl group is lying in perpendicular plane respect to the pyrimidine ring. The dihedral angle N16C15C20C21 is $171.89^\circ \approx 180^\circ$, also the dihedral angle, C15C20C21C22 is $176.18^\circ \approx 18^\circ$, these values confirm that the benzylidene ring is lying in the same plane of the imidazole ring, also the values of the dihedral angles C26C21C20C15 and C21C20C15C14 are $7.63^\circ \approx 0.00^\circ$ and $4.55^\circ \approx 0.00^\circ$ as shown in Figure 10. The main observation from the dihedral angles of the optimized geometrical structure of the compound **12** that the two oxygen atoms O7 and O8 are lying in the same plane, while the oxygen atom O18 is lying out of this plane, one of these atoms can be participate in the chelation as donor atom with any acceptor atom. The calculated Mulliken charge density over these oxygen atoms helps us to detect which of these oxygen atoms can be behaved as active site in bonding with acceptor atom in docking calculations.

There is building up of charge density on the all hetero atoms nitrogen and oxygen atoms, the highest negative charged atoms are O7 and O8, -0.442 and -0.432 , while the negative charges on nitrogen atoms of the pyrimidine ring, N4 and N6 are -0.328 and -0.208 , also the negative charges on the nitrogen atoms of imidazole ring, N13 and N16 are -0.135 and -0.385 . These values of charges confirmed that the oxygen atoms can be participate in bonding with any acceptor more than nitrogen atoms involved in the compound **12**, so the oxygen atom, O7 can be considered as active site in this compound and can bond through it with any acceptor as shown in the docking calculations. The charge density on other atoms less negative than these atoms as listed in Table S1. The energy of the compound **12**, 6-amino-5-(4-benzylidene-2-methyl-5-oxo-4,5-dihydro-1H-imidazol-1-yl)-1-ethylpyrimidine-2,4(1H,3H)-dione is $-141,856.224$ kcal/mol, heat of formation is -8661.756 kcal/mol and slightly high dipole $8.326D$. From the value of energy we found that this compound has higher energy value greater than the compound **3**, which has lower energy and lower dipole moment.

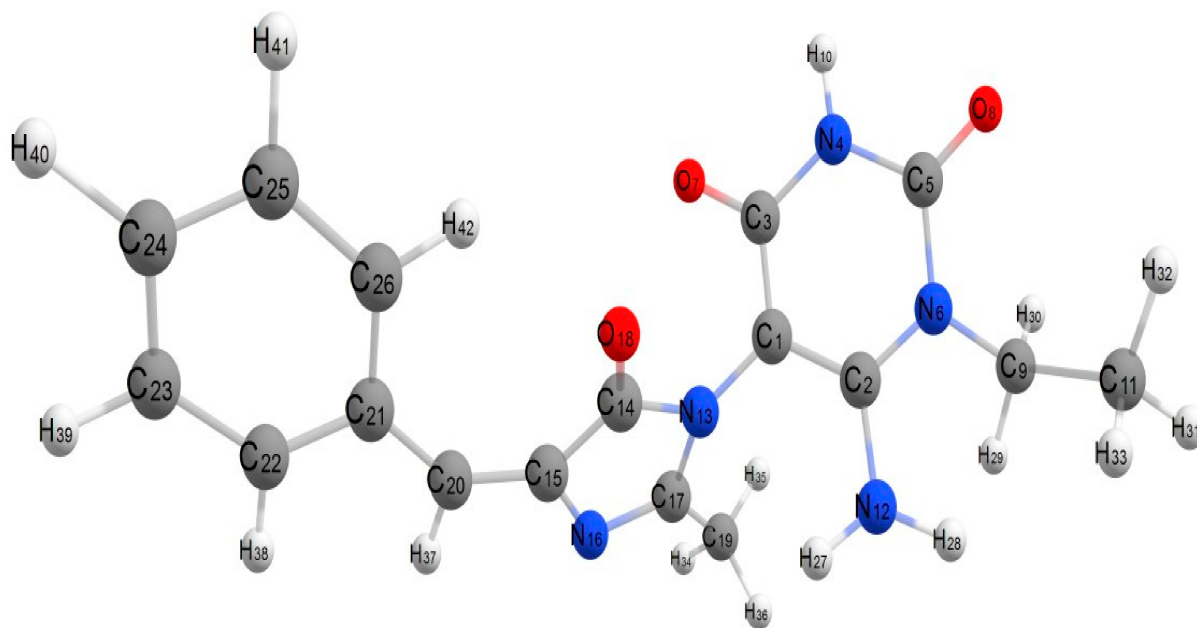


Figure 10. Optimized geometrical structure of compound (12), 6-amino-5-(4-benzylidene-2-methyl-5-oxo-4,5-dihydro-1H-imidazol-1-yl)-1-ethylpyrimidine-2,4(1H,3H)-dione by using DFT calculations.

6-Amino-5-(4-benzylidene-2-methyl-5-oxo-4,5-dihydro-1H-imidazol-1-yl)-1-methyl-2-thioxo-2,3-dihydropyrimidin-4(1H)-one, compound **13**

This compound is similar to the compound (12) with replacement of the C=O of the pyrimidine ring with C=S, the bond length C3-N4 is and C5-N4 are 1.369 and 1.383 Å, there is a single bond characters C and N atoms in the pyrimidine ring [48], also the bond lengths of N12-C16, C13-N12 and C14-N15 of the imidazole ring are 1.352, 1.348 and 1.359 Å, these values reflect that these bonds have single bond characters, while the bond distance of C16-N15 of the imidazol ring is 1.339 Å, whereas this bond has double bond characters [48] as shown in the (Figure 11). All calculated bond distances, bond angles and dihedral angles between the atoms of the compound **13** are given in (Table S2). The C5-S8 bond length is 1.692 Å [53] and the C3-O7 bond length is 1.209 Å [50], while the C13-O17 bond length is 1.208 Å [50].

There is no significant difference between the structure of this compound and compound (12), the benzylidene ring and dihydropyrimidine ring are lying in the same plane, the dihedral angles C13C14C19C20 and C14C19C20C25 are $6.42^\circ \approx 0.00^\circ$ and $11.35^\circ \approx 0.00^\circ$, these values confirm that the benzylidene ring and dihydropyrimidine ring are lying in the same plane, while the dihedral angle C3C1N12C13 is -49.18° , so the imidazol ring is lying out of the plane occupied by others two rings, as shown in the (Figure 11). The dihedral angles C2N6C5S8 is -153.03° and O7C3C1C2 is 169.59° , which confirms that the O7 and S8 are lying in the same plane of the nitrogen atom N4 of dihydropyrimidin ring, while the dihedral angle O17C13N12C1 of the imidazol ring is $79.9^\circ \approx 90.0^\circ$, so the oxygen atom O17 is lying away from the other plane occupied by O7 and S8. In this compound there are many hetero atoms can behave as active donating site, the active donating site can be detected from the value of accumulated charges spreading over hetero atoms.

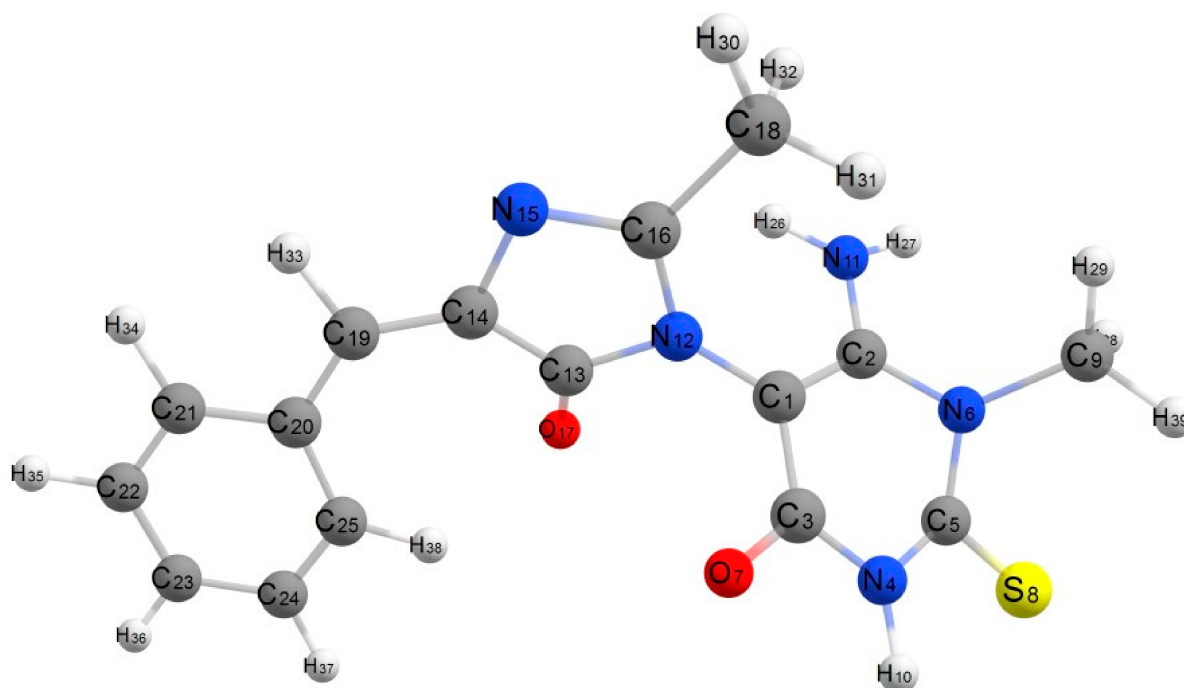


Figure 11. Optimized geometrical structure of compound **13**, 6-amino-5-(4-benzylidene-2-methyl-5-oxo-4,5-dihydro-1H-imidazol-1-yl)-1-methyl-2-thioxo-2,3-dihydropyrimidin-4(1H)-one by using DFT calculations.

There is building up of negative charge density on the nitrogen atoms, oxygen atoms and sulfur atom in the compound **13**, 6-amino-5-(4-benzylidene-2-methyl-5-oxo-4,5-dihydro-1H-imidazol-1-yl)-1-methyl-2-thioxo-2,3-dihydropyrimidin-4(1H)-one, oxygen atom, O7 and sulfur atom, S8 are the highest charged atoms, -0.413 and -0.616 , while nitrogen atoms have lower charge densities less than oxygen atoms, the charge accumulated on N4 (-0.389) and N6 are (-0.261) and (-0.163), while the charge on the N12 and N15 are -0.134 and -0.347 . The charge density on other atoms less negative than these atoms as listed in Table S3, so that the compound **13** have a power full chelating sites oxygen atom, O7 and sulfur atom S8 more than others compounds, from the optimized structure the bonding of compound **13** favors bonding through the oxygen atom O7 not through sulfur atom S8, the dihedral angles C2N6C5S8 and C9N6C5S8 are 153.03° and -43.49° , these values reflected that sulfur atom is not completely planer, while the dihedral angles N12C1C3O7 and O7C3C1C2 are $-13.93^\circ \approx 00.0^\circ$ and $169.59^\circ \approx 180.0^\circ$, these values reflected that oxygen atom O7 is nearly planer, so oxygen atom, O7 is considered as active site in bonding with acceptor atom. The energy of the compound **13** is $-132,805.565$ kcal/mol, heat of formation is -8086.449 kcal/mol and highly dipole 8.586 D more than others previous compounds.

6-Amino-5-((4-(dimethylamino)benzylidene)amino)-1-ethylpyrimidine-2,4(1H,3H)-dione, compound (**16**)

This compound is more energetic than all studied compound, the energy of it is $-123,990.259$ kcal/mol, so this compound is less stable than others. The heat of formation of this compound is -8026.826 kcal/mol, the value of dipole moment is 6.051 D, this value is slightly high, this value is greater than dipole moment of the compound **3** and less than compounds **12** and **13**, this result attributed to the presence of C25=N24 bond as bridge between the two aromatic rings, which facilitates the rotation of any aromatic ring around it. All geometrical parameters of the compound **16**, 6-amino-5-((4-(dimethylamino)benzylidene)amino)-1-ethylpyrimidine-2,4(1H,3H)-dione, bond lengths, bond angles and dihedral angles are given in (Table S3). The bond length C16-N15 is 1.379 Å is longer slightly than bond length of C14-N15 is 1.376 Å, from the values of bond lengths, C13-

N17 and N17-C16, there is a single bond characters C and N atoms [49], the bond length of C25-N24 is 1.347 Å, whereas this bond has a double bond characters [49]. Detailed analysis of corresponding bond lengths in various hetero cyclic compounds were given elsewhere [50]. The C14-O18 and C16-O19 bond lengths of the pyrimidine ring are 1.211 Å and 1.208 Å [50].

As seen in (Figure 12) of the optimized geometrical structure of the compound 16, The compound is non planar and there are two planes each of them is perpendicular respect to each other, the dihedral angles C25N24C12C14 and C25N24C12C13 are 50.26° and −131.88°, where the values are neither zero nor 180°, these values reflected that the plane occupied by pyrimidine ring is perpendicular with the plane occupied by benzylidene ring, the dihedral angle C13N17C20C22 is −83.59° ≈ 90°, this value confirms that the terminal ethyl group is lying in plane perpendicular with the plane occupied by pyrimidine ring. Also, the value of dihedral angle of C5N6C9C11 is 90.54° ≈ 90°, this value confirms that the terminal ethyl group is lying in perpendicular plane respect to the pyrimidine ring. The dihedral angles C20N17C16O19 and N24C12C14O18 are 1.65° ≈ 0.00° and 0.10° ≈ 0.00° as shown in (Figure 12). The main observation from the dihedral angles of the optimized geometrical structure of the compound 16 that the two oxygen atoms O18 and O19 are lying in the same plane, one of them can be considered as an active site in this compound. The calculated Mulliken charge density over these two oxygen atoms can be used to detect which of them can be used in bonding with acceptor atom in docking calculations.

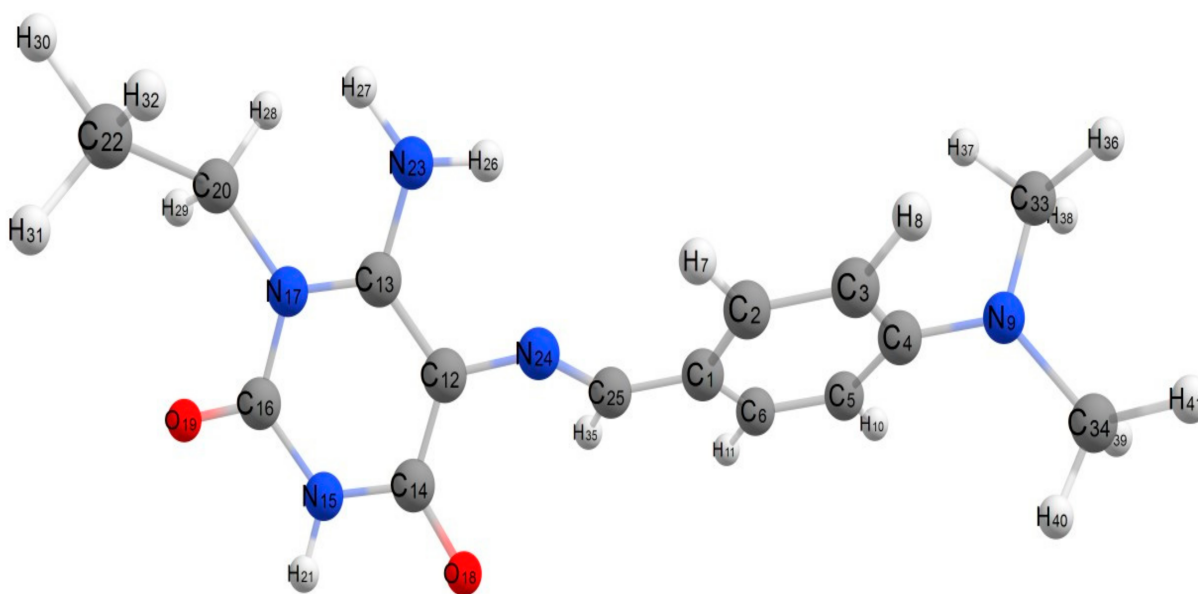


Figure 12. Optimized geometrical structure of compound (16), 6-amino-5-((4-(dimethylamino) benzylidene)amino)-1-ethylpyrimidine-2,4(1H,3H)-dione by using DFT calculations.

There is building up of charge density on the all hetero atoms nitrogen and oxygen atoms, the highest negative charged atoms are O18 and O19, −0.448 and −0.459, while the negative charges on nitrogen atoms of the pyrimidine ring, N15 and N17 are −0.429 and −0.203, also the negative charge on the terminal nitrogen atom of amino group, N9 is −0.437. These values of charges confirmed that the oxygen atom, O18 can behave as an active site in the compound 16 and can bond through it with any acceptor as shown in the docking calculations. The charge density on other atoms less negative than these atoms as listed in (Table S4).

2.5.2. Charge Distribution Analysis

The charge distribution analysis on the optimized geometry configuration of the all studied compounds was made on the basis of natural population analysis (NPA). The charge distribution on the hetero atoms, nitrogen, oxygen and sulfur of the different studied

compounds indicates the presence of a net negative pole attributed to the presence of polar atoms beside the high degree of planarity of these molecules, as a result the molecules are a slightly high dipole in case of compound **3**, 8.586D, while compound **2** has slightly weak dipole, 3.078D less than others compounds. There is building up of charge density on the donating oxygen, nitrogen and sulfur atoms involved in the studied compounds. All calculated parameters, dipole moment, Mulliken charges and total energies are given in (Table 6). From the factors affecting on the degree of stability of these compounds is the value of the total energy and distribution charges over all atoms in compounds. From the values of energies, the compound **3**, N-(1-(3-benzyl-2,6-dioxo-2,3,6,7-tetrahydro-1H-purin-8-yl)-2-(4-chlorophenyl)vinyl)acetamide is considered as more stable than others, with more negative energy value less than second compound **12** by 30,203.498 kcal/mol, while the third compound in stability is **13**, the difference in energy between it and the first compound **3** is 39,254.157 kcal/mol. The energy difference between the less stable compound **16** and the most stable compound **3** is 48,069.463 kcal/mol.

Table 6. Calculated charges on donating sites and energy values (HOMO, LUMO, Energy gap ΔE /eV, hardness (η), global softness (S), electro negativity (χ), absolute softness (σ), chemical potential (Pi), global electrophilicity (ω) and additional electronic charge (ΔN_{\max}) of the studied four compounds by using DFT calculations.

Parameters	Compound 3	Compound 12	Compound 13	Compound 16
HOMO, H	-0.319	-0.321	-0.315	-0.309
LUMO, L	-0.237	-0.245	-0.254	-0.237
I = -H	0.319	0.321	0.315	0.309
A = -L	0.237	0.245	0.254	0.237
$\Delta E = L - H$	0.082	0.067	0.061	0.072
$\eta = (I - A)/2$	0.041	0.034	0.031	0.036
$\chi = -(H - L/2)$	0.278	0.283	0.285	0.237
$\sigma = 1/\eta$	24.390	29.412	32.258	27.778
$S = 1/2 \eta$	12.195	14.706	16.129	13.889
Pi = - χ	-0.278	-0.283	-0.285	-0.237
$\omega = (Pi)^2/2 \eta$	0.942	1.178	1.310	0.780
$\Delta N_{\max} = \chi/\eta$	6.780	8.324	9.194	6.583

(I) is ionization energy. (A) is an electron affinity.

2.5.3. Molecular Orbitals and Frontier

Molecular orbitals play also an important role in the electric properties, as well as in UV-Vis [54]. An electronic system with smaller values of HOMO-LUMO gap should be more reactive than one having a greater energy gap [55]. The energy gap, ΔE of the studied compounds varied between 0.061 for Compound **13** which more reactive and 0.082 eV for compound **3** which less reactive, so electron movement between these orbitals could be easily occur by decreasing the value of energy gap, so that there is a peak around 250 nm in the UV-Vis spectra for all studied compounds as shown in UV-Vis spectra for all studied compounds. The energy gap is closely associated with the reactivity and stability of the executed compounds and shows the nature of the compound with low kinetic stability and slightly high chemical reactivity. On the other hand, the adjacent orbitals are often closely spaced on the frontier region.

The nodal properties of molecular orbitals of studied complexes in Figure 13 are illustrative and suggest orbital delocalization, strong orbital overlap, and low number of nodal planes. The energy difference between HOMO and LUMO (energy gap, ΔE) for the all studied compounds varied according to the composition of each compound or the type of substitutions as shown in (Table 7), and (Figure 13), shows the isodensity surface plots of HOMO and LUMO for the studied compounds. Hard molecules have high the HOMO-LUMO gap, and soft molecules have smaller HOMO-LUMO gap [56]. The values of η and ΔE (HOMO-LUMO) are given in (Table 7). It is obvious that the compound **3** is considered as most hard with η equals to 0.041, and compound **13** is considered as less

hard molecule with η equals to 0.031, also the electronic transition within the compounds is easy as indicated from the ΔE . There are some quantum chemical parameters depending upon the energy values of HOMO and LUMO were calculated as global softness (S), electro negativity (χ), absolute softness (σ), chemical potential (μ), global electrophilicity (ω) and additional electronic charge (ΔN_{\max}) of the all studied compounds. From these values, the compound **3** is absolute more soft according to the ($\sigma = 24.390$ eV), while the compound **13** is treated as less soft compound ($\sigma = 32.258$ eV).

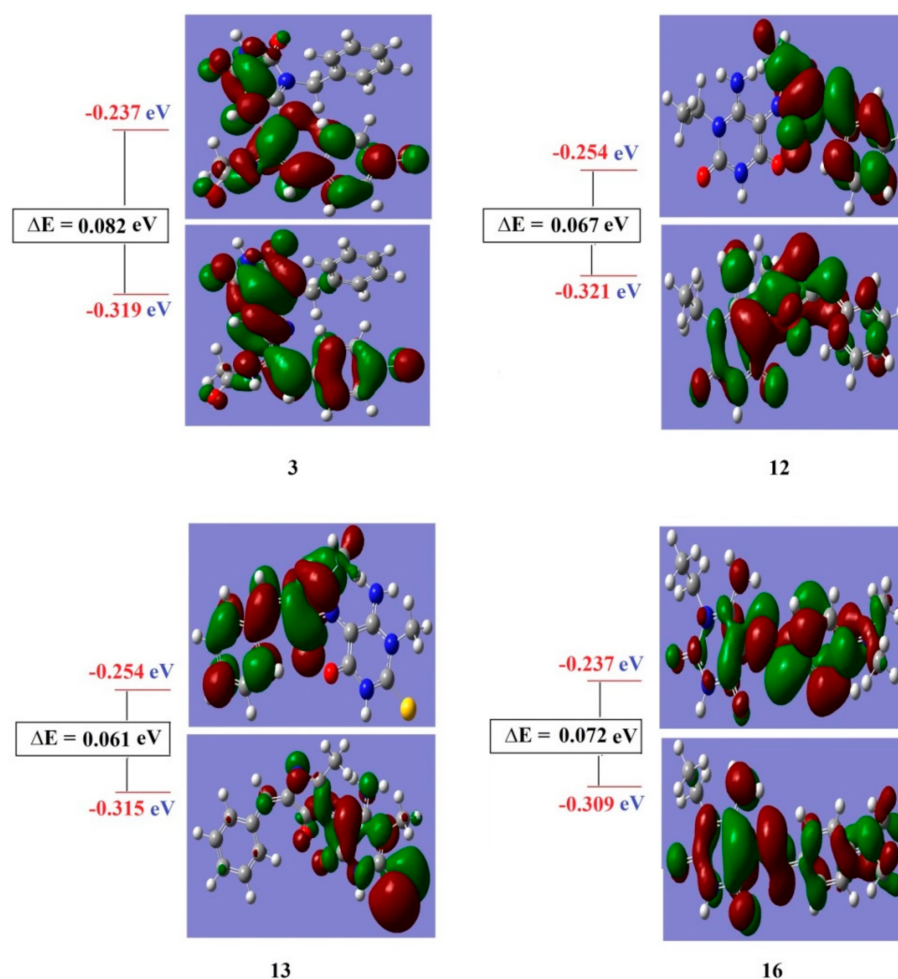


Figure 13. Molecular orbital surfaces and energy levels of all studied compounds, **3**, **12**, **13** and **16** by using DFT calculations.

As seen in Figure 13, the electron density of HOMO, Ψ 113 of the compound **3** is delocalized over all atoms with highly percent on the two oxygen atoms of the C=O groups of the 2,6-dioxopurine ring with percent 55.5%, with spreading of the remaining percentage on the remaining components, with 20.2% on the acetamide group, 15.4% on the chlorophenyl ring, 7.9% on the vinyl group and finally 1% on the benzyl group. The LUMO, Ψ 114, the electron density delocalized over all atoms of compound **3**, the most percent (53.7%) is localized on the 2,6-dioxopurine ring with spreading of remaining percentage over the remaining components except benzyl group with 0.0%, as given in (Table 8). Also the HOMO, Ψ 89 of the compound **12**, the electron density delocalized over all atoms, the most percent (61.2%) is localized on the 2-methyl-5-oxoimidazol ring and 25.6% on the 2,4-dioxo-6-aminopyrimidine ring with small percent 13.2% on the benzylidene ring, without any percent on the terminal ethyl group. The LUMO, Ψ 90 of the compound **12**, the electron density delocalized over all atoms, the most percent (51.9%) is localized on the 2,4-dioxo-6-aminopyrimidine ring and 48.1% on the benzylidene ring only.

Table 7. Composition of the frontier molecular orbital for studied the compounds **3**, **12**, **13** and **16** by using DFT/B3LYP/Cep-31G.

	Compound 3			Compound 12	
	H	L		H	L
2,6-dioxopurine ring C10, N11, C16-O24	55.5%	53.7%	2,4-dioxo-6-aminopyrimidine ring C1-O8, N12	25.6%	0.0%
Chlorophenyl ring C1-C17	15.4%	21.8%	2-methyl-5-oxoimidazol ring N13-C19	61.2%	51.9%
Vinyl group C8-C9	7.9%	15.9%	Benzylidene ring C20-C26	13.2%	48.1%
acetamide group N12-C15	20.2%	8.6%	Ethyl group C9, C11	0.0%	0.0%
Benzyl group C25-C31	1%	0.0%			
	Compound 13			Compound 16	
	H	L		H	L
2-thio-4-oxo-6-aminopyrimidine ring C1-S8, N11	56.3%	0.0%	2,4-dioxo-6-aminopyrimidine ring C13-O19, N23	41.3%	19.5%
2-methyl-5-oxoimidazol ring N12-C18	41.9%	52.7%	dimethylaminobenzylidene ring C1-N9, C33-C34	33.6%	58.7%
Benzylidene ring C19-C25	1.8%	31.4%	Amino group N24-C25	25.1%	21.8%
Methyl group C9	0.0%	15.9%	Ethyl group C20, C22	0.0%	0.0%

The HOMO of the compound **13**, Ψ 89, the electron density localized over 2-thio-4-oxo-6-aminopyrimidine ring with percent (56.3%) and 41.9% on the 2-methyl-5-oxoimidazol ring, with small percent on benzylidene ring (1.8%) and without any percent on the terminal methyl group. The LUMO, Ψ 90, the electron density delocalized over all atoms, the most percent (52.7%) is localized on the 2-methyl-5-oxoimidazol ring and 31.4% on the benzylidene ring with small percent on the terminal methyl group (15.9%), while 0.0% on the 2-thio-4-oxo-6-aminopyrimidine.

In compound **16**, the HOMO, Ψ 80, the electron density delocalized over all atoms of this compound with percent (41.3%) on the 2,4-dioxo-6-aminopyrimidine group, 33.6% on the dimethylaminobenzylidene ring and 25.1% on the Amino group with 0.0% on the terminal ethyl group. The LUMO, Ψ 81, the electron density delocalized over all atoms in this compound with 58.7% localized on the dimethylaminobenzylidene ring, 21.8% on the amino group and 19.5% on the 2,4-dioxo-6-aminopyrimidine ring without any percent on the ethyl group 0.0%. The variation in the distribution of electron densities on the components of HOMO and LUMO for each compound play important role in the variation of electronic transitions occurred in compounds and effect on the degree of biological effect of them.

Table 8. Computed excitation energies (eV), electronic transition configurations and wave lengths (nm) of the obtained stable compounds; **3** and **12** by using B3LYP/Cep-31G for the, ($f \geq 0.001$) f = oscillator strengths compared with experimental data of UV-Visible spectra, λ_{\max} , nm.

Compound	eV	nm	Major Contributions	Assignment	λ_{\max} , nm
3	4.9546	250.24	H-11 \rightarrow L(4.5%), H-11 \rightarrow L + 6(2.9%), H \rightarrow L(4.9%), H-7 \rightarrow L(3.2%), H-5 \rightarrow L(34.5%), H-3 \rightarrow L(3.7%), H-1 \rightarrow L(14.7%), H \rightarrow L(4.4%)	π - π *	265
	4.7874	258.98	H-11 \rightarrow L (7.8%), H-10 \rightarrow L (2.5%), H-5 \rightarrow L (2.8%), H-1 \rightarrow L (78.4%), H \rightarrow L(4.6%), H \rightarrow L + 1(3.6%)	π - π *	275
	4.4144	280.86	H-11 \rightarrow L + 7 (4.9%), H-10 \rightarrow L + 6 (14.1%), H-10 \rightarrow L + 7 (41.8%), H-7 \rightarrow L + 7 (6.7%), H-6 \rightarrow L + 6 (9.6%), H-6 \rightarrow L + 7 (26.7%)	n - π *	290
	4.0996	302.43	H-9 \rightarrow L (5.2%), H-9 \rightarrow L + 5 (61.6%), H-9 \rightarrow L + 6 (21.3%), H-9 \rightarrow L + 7 (2.7%), H-8 \rightarrow L + 5(6.3%), H-8 \rightarrow L + 6 (2.8%)	π - π *	305
	3.4797	356.3	H-11 \rightarrow L + 2 (5.3%), H-10 \rightarrow L (6.3%), H-10 \rightarrow L + 1 (10.4%), H-6 \rightarrow L (22.9%), H-6 \rightarrow L + 1 (38.3%), H-6 \rightarrow L + 7 (8.8%), H-6 \rightarrow L + 10 (7.8%)	n - π *	368
	3.2847	377.47	H-1 \rightarrow L (4.5%), H \rightarrow L(93.4%)	π - π *	383
	4.7935	258.65	H-8 \rightarrow L + 1 (2.4%), H-1 \rightarrow L + 1 (54.4%), H \rightarrow L + 1 (43%)	π - π *	269
	4.4183	280.61	H-6 \rightarrow L (5.8%), H-4 \rightarrow L (9.8%), H-3 \rightarrow L (8.6%), H-2 \rightarrow L(2.7%), H-1 \rightarrow L(72.8%)	π - π *	278
	4.3485	285.12	H-9 \rightarrow L + 3 (20.5%), H-9 \rightarrow L + 4 (12.4%), H-8 \rightarrow L + 3 (7.6%), H-8 \rightarrow L + 4 (4%), H-7 \rightarrow L + 3 (27.3%), H-3 \rightarrow L + 4 (16.6%), H-5 \rightarrow L + 3 (7%), H-5 \rightarrow L + 4 (4.2%)	n - π *	300
	4.0172	308.64	H-10 \rightarrow L (5%), H-8 \rightarrow L (35.2%), H-8 \rightarrow L + 3 (3.3%), H-8 \rightarrow L + 4 (7.3%), H-3 \rightarrow L (15.4%), H-3 \rightarrow L + 3 (8.5%), H-3 \rightarrow L + 4 (8.2%), H-3 \rightarrow L + 5 (7%)	n - π *	315
12	3.8482	322.23	H-6 \rightarrow L + 1 (6.1%), H-5 \rightarrow L + 1 (35.8%), H-5 \rightarrow L + 3 (13.5%), H-5 \rightarrow L + 6 (13.6%), H-4 \rightarrow L + 1 (18.3%), H-4 \rightarrow L + 3 (6.3%), H-4 \rightarrow L + 6 (6%)	n - π *	322
	3.7319	332.23	H \rightarrow L (100%)	π - π *	338
	3.6207	342.43	H-8 \rightarrow L (14.5%), H-8 \rightarrow L + 5 (8.9%), H-6 \rightarrow L (3.3%), H-5 \rightarrow L(11.7%), H-5 \rightarrow L + 5 (3%), H-4 \rightarrow L (5.7%), H-3 \rightarrow L (36.7%), H-3 \rightarrow L + 5 (3.5%)	n - π *	350

2.5.4. Excited State

The TD-DFT at the B3LYP level by using G98W program proved to give accurate description of the UV-vis. spectra [57,58]. Time-dependent density functional response theory (TD-DFT) has been recently reformulated [59] to compute discrete transition energies and oscillator strengths and has been applied to a number of different atoms and molecule. Bauernschmitt and Ahlrichs [60] included hybrid functional proposed in the calculation of the excitation energies. These hybrid methods typically constitute a considerable improvement over conventional Hartree-Fock (HF) based methods. In this work, the optimized geometry was calculated and was used in all subsequent calculations; the wave functions of SCF MOs were explicitly analyzed. The calculated wave functions of the different MOs reflect and suggest the fraction of the different fragments of the compounds contributing to the total wave functions of different states. The results indicate that there is an extent of electron delocalization in the different molecular orbitals.

The electronic transition could be described as a mixed $n \rightarrow \pi^*$ and $\pi \rightarrow \pi^*$ transitions. The energies of HOMO and LUMO states for the all studied compounds are listed in

Table 8. The HOMO can perform as an electron donor and the LUMO as the electron acceptor in reaction profile.

Table 8 indicates that there are six excited states are involved in case of compound **3**, N-(1-(3-benzyl-2,6-dioxo-2,3,6,7-tetrahydro-1H-purin-8-yl)-2-(4-chlorophenyl)vinyl)acetamide, the first excited state results from a combination eight transitions, H-11 \rightarrow L(4.5%), H-11 \rightarrow L + 6(2.9%), H \rightarrow L(4.9%), H-7 \rightarrow L(3.2%), H-5 \rightarrow L(34.5%), H-3 \rightarrow L(3.7%), H-1 \rightarrow L(14.7%), H \rightarrow L(4.4%), this excited state assigned to π - π^* at 250.24 nm and 4.9546 eV, this theoretical value agree with experimental peak at 265 nm. The second excited state result from the interaction between electronic configurations which represent $\pi \rightarrow \pi^*$ transition. This is transition results from H-11 \rightarrow L (7.8%), H-10 \rightarrow L (2.5%), H-5 \rightarrow L (2.8%), H-1 \rightarrow L (78.4%), H \rightarrow L (4.6%), H \rightarrow L + 1(3.6%), the energy of transition is 4.2308 eV, calculated wave length is 258.98nm and can be observed experimentally at 275 nm. The third excited state is assigned to $n \rightarrow \pi^*$ transition, represents a transition appears at 280.861 nm and 4.4144 eV, H-11 \rightarrow L + 7 (4.9%), H-10 \rightarrow L + 6 (14.1%), H-10 \rightarrow L + 7 (41.8%), H-7 \rightarrow L + 7 (6.7%), H-6 \rightarrow L + 6 (9.6%), H-6 \rightarrow L + 7 (26.7%). The fourth excited state at 302.43 nm and 4.0996 eV, results as H-9 \rightarrow L (5.2%), H-9 \rightarrow L + 5 (61.6%), H-9 \rightarrow L + 6 (21.3%), H-9 \rightarrow L + 7 (2.7%), H-8 \rightarrow L + 5(6.3%), H-8 \rightarrow L + 6 (2.8%) and assigned to π - π^* . The fifth excited state at 356.3 nm and 3.4797 eV, results as H-11 \rightarrow L + 2 (5.3%), H-10 \rightarrow L (6.3%), H-10 \rightarrow L + 1 (10.4%), H-6 \rightarrow L (22.9%), H-6 \rightarrow L + 1 (38.3%), H-6 \rightarrow L + 7 (8.8%), H-6 \rightarrow L + 10 (7.8%) and assigned to n - π^* . The sixth excited state is assigned to $\pi \rightarrow \pi^*$ transition, represented at 377.47nm and 3.2847 eV, H-1 \rightarrow L (4.5%), H \rightarrow L (93.4%). All calculated transitions agree with experimental data obtained from the UV-Visible spectra as given in Table 8. Also, in compound **13**, 6-amino-5-(4-benzylidene-2-methyl-5-oxo-4,5-dihydro-1H-imidazol-1-yl)-1-ethylpyrimidine-2,4(1H,3H)-dione, the first excited state assigned to an $\pi \rightarrow \pi^*$ transition at 258.65 nm and 4.7935 eV, this transition represented by H-8 \rightarrow L + 1 (2.4%), H-1 \rightarrow L + 1 (54.4%), H \rightarrow L + 1 (43%). The second excited state is assigned to $\pi \rightarrow \pi^*$ transitions, represents a transitions H-6 \rightarrow L (5.8%), H-4 \rightarrow L (9.8%), H-3 \rightarrow L (8.6%), H-2 \rightarrow L (2.7%), H-1 \rightarrow L (72.8%) which observed around 280.61 nm and 4.4183 eV. The third excited state is assigned to $n \rightarrow \pi^*$ transition, represents a transition appears at 285.12 nm and 4.3485 eV, H-9 \rightarrow L + 3 (20.5%), H-9 \rightarrow L + 4 (12.4%), H-8 \rightarrow L + 3 (7.6%), H-8 \rightarrow L + 4 (4%), H-7 \rightarrow L + 3 (27.3%), H-3 \rightarrow L + 4 (16.6%), H-5 \rightarrow L + 3 (7%), H-5 \rightarrow L + 4 (4.2%). The fourth excited state at 308.64 nm and 4.0172 eV, results as H-10 \rightarrow L (5%), H-8 \rightarrow L (35.2%), H-8 \rightarrow L + 3 (3.3%), H-8 \rightarrow L + 4 (7.3%), H-3 \rightarrow L (15.4%), H-3 \rightarrow L + 3 (8.5%), H-3 \rightarrow L + 4 (8.2%), H-3 \rightarrow L + 5 (7%) and assigned to n - π^* transitions. The fifth excited state is assigned to $n \rightarrow \pi^*$ transition, represents a transition appears at 322.23 nm and 3.8482 eV, H-6 \rightarrow L + 1 (6.1%), H-5 \rightarrow L + 1 (35.8%), H-5 \rightarrow L + 3 (13.5%), H-5 \rightarrow L + 6 (13.6%), H-4 \rightarrow L + 1 (18.3%), H-4 \rightarrow L + 3 (6.3%), H-4 \rightarrow L + 6 (6%). The sixth excited state at 332.23 nm and 3.7319eV, results as one transition only H \rightarrow L (100%) and assigned to π - π^* transitions. The seventh excited state at 342.43 nm and 3.6207 eV, results as H-8 \rightarrow L (14.5%), H-8 \rightarrow L + 5 (8.9%), H-6 \rightarrow L (3.3%), H-5 \rightarrow L (11.7%), H-5 \rightarrow L + 5 (3%), H-4 \rightarrow L (5.7%), H-3 \rightarrow L (36.7%), H-3 \rightarrow L + 5 (3.5%) and assigned to n - π^* transitions.

As given in Table 8, the experimental data of the UV-Visible spectra of compound **3**, **12** are compared nicely with calculated excited states.

In compound **13**, there are five peaks obtained in spectra, while theoretically there are nine transitions can be observed as given in (Table S4). The first peak obtained at 267 nm, this peak is composed of two theoretical transition states overlapped together at 260.77 nm and 263.14 nm, these transitions are assigned to π - π^* . The second peak obtained at 290 nm, we found that this peak is consist of two overlapped excited states at 284.13 nm and 284.13 nm, the first one is assigned to π - π^* and the second is assigned to n - π^* transitions. Also, the third peak observed at 322 nm is composed of three overlapped transition states at 288.71 nm, 326.03 and 328.13 nm, the first and third transition states assigned to π - π^* transitions, while the second transition states assigned to n - π^* transition. The fourth peak observed experimentally at 339 nm and this peak is agree theoretically

with these electronic transitions, H-10 \rightarrow L (2.8%), H-9 \rightarrow L (12.7%), H-9 \rightarrow L + 4 (8.1%), H-6 \rightarrow L (9.7%), H-6 \rightarrow L + 5 (8.5%), H-5 \rightarrow L (4.1%), H-5 \rightarrow L + 5 (10.7%), H-4 \rightarrow L (82.6%), H-2 \rightarrow L + 2 (17.3%), which obtained at 339.43 nm and 3.7876 eV, this transition is assigned to $n\text{-}\pi^*$. The last peak observed experimentally at 357nm, this peak can be represented by these transitions, H-2 \rightarrow L + 1 (3.2%), H-3 \rightarrow L (7.8%), this excited state is assigned to $n\text{-}\pi^*$ transition, the theoretical wave length corresponding with excited state is 359.12 nm with energy equals to 3.4525 eV.

In (Table S5), the number of excited states involved in compound **16** are five transition states, there are four of them are assigned to $\pi\text{-}\pi^*$, which can be observed at 249.89, 313.44, 335.42 and 365.71nm, while fourth excited state is assigned to $n\text{-}\pi^*$, this transition can be observed at 278.83 nm.

3. Material and Methods

3.1. Chemistry

3.1.1. Materials and Instruments

All melting points were determined by an Electrothermal Mel.-Temp. II apparatus and were uncorrected. Element analyses were performed at Regional Center for Mycology and Biotechnology at Al-Azhar University. The infrared (IR) spectra were recorded using potassium bromide disc technique on Nikolet IR 200 FT IR (Perkin-Elmer, Akron, OH, USA). Mass spectra were recorded on DI-50 unit of Shimadzu GC/MS-QP 5050A at the Regional Center for Mycology and Biotechnology at Al-Azhar University. The proton nuclear magnetic resonance ($^1\text{H-NMR}$) spectra were recorded on Bruker 400 MHz Spectrometer and $^{13}\text{C-NMR}$ spectra were run at 125 MHz in dimethylsulfoxide (DMSO-*d*₆) and TMS as an internal standard, Applied Nucleic Acid Research Center, Zagazig University, Egypt. All new compounds gave corresponding elemental analyses (C, H, N, typically $\pm 0.3\%$). All reactions were monitored by TLC using precoated plastic sheets silica gel (Merck 60 F₂₅₄) and spots were visualized by irradiation with UV light (254 nm). The used solvent system was chloroform: methanol (9:1) and ethyl acetate: toluene (1:1).

3.1.2. Synthetic Procedures

5,6-diaminouracils **1a-e**. These compounds were prepared according to a reported method [25,38,39]. 4-arylideno-5(4*H*)-1,3-oxazolones (**2a-c**) These compounds were prepared according to a reported method [40–43].

3.1.3. N-Substituted-8-purinyl-2-(arylvinyl)acetamides **3-5**

General method: A mixture of 5,6-diaminouracils (0.75 mmol) and the appropriate azalactone derivatives (0.75 mmol) in acetic acid (3 mL) was heated in a water bath for 1 h. The formed precipitate was filtered, washed with ethanol and recrystallized from DMF/ethanol (2:1).

3.1.4. N-(1-(3-Benzyl-2,6-dioxo-2,3,6,7-tetrahydro-1H-purin-8-yl)-2-(4-chlorophenyl)vinyl) acetamide (**3**)

Yield: 80%; m.p. = 220 °C; IR (KBr) ν_{max} (cm⁻¹): 3291, 3194 (NH), 3032 (CH arom.), 2924 (CH aliph.), 1705, 1651 (C=O), 1581 (C=N), 1512 (C=C), 833 (*p*-substituted phenyl); $^1\text{H NMR}$ (DMSO-*d*₆) δ 12.71 (s, 1H, NH), 10.69 (s, 1H, NH), 9.48 (s, 1H, NH), 8.13–8.10 (d, *J* = 8.4 Hz, 1H, arom.), 7.62–7.58 (dd, *J* = 8.4 Hz, 2H arom.), 7.47–7.45 (d, *J* = 8.4 Hz, 2H, arom.), 7.38–7.31 (m, 3H, arom.), 7.29–7.19 (m, 1H, arom.), 6.56 (s, 1H), 5.09 (s, 2H), 1.90 (s, 3H, CH₃); $^{13}\text{C NMR}$ (DMSO-*d*₆): δ 171.88, 167.50, 161.56, 154.65, 151.54, 136.48, 135.19, 133.33, 132.36, 132.31, 129.88, 129.83, 128.58, 127.66, 127.39, 88.14, 45.46, 23.54; MS: *m/z* (%) = *M* + 2, 437 (55), *M*⁺, 435 (34), 430 (58), 426 (77), 425 (74), 400 (55), 347 (94), 320 (100), 313 (65), 279 (70), 253 (66), 171 (54), 162 (97), 54 (74), 53 (98); Anal. calcd. for C₂₂H₁₈ClN₅O₃ (435.87): C, 60.62; H, 4.16; N, 16.07; Found: C, 60.76; H, 4.28; N, 16.32.

3.1.5. N-(2-(4-Chlorophenyl)-1-(3-methyl-6-oxo-2-thioxo-2,3,6,7-tetrahydro-1H-purin-8-yl) vinyl) acetamide (4)

Yield: 74%; m.p.=314 °C; IR (KBr) ν_{\max} (cm⁻¹): 3309, 3201 (NH), 3039 (CH arom.), 2924 (CH aliph.), 1666, 1620 (C=O), 1550 (C=N), 1489 (C=C), 818 (*p*-substituted phenyl); ¹H NMR (DMSO-d₆): δ 12.49 (s, 1H, NH), 12.04 (s, 1H, NH), 9.67 (s, 1H, NH), 7.99–7.97 (d, *J* = 8.0 Hz, 2H), 7.62–7.60 (d, *J* = 8.0 Hz, 2H), 6.79 (s, 1H), 3.73 (s, 3H), 1.93 (s, 3H) ppm.; ¹H NMR (DMSO-d₆): δ 175.76, 172.87, 158.90, 158.32, 154.78, 151.16, 145.10, 134.12, 129.76, 124.18, 107.12, 92.64, 37.12, 23.37 ppm.; MS: *m/z* (%) = *M* + 2, 377 (36), *M*+, 375 (35). 340 (80), 332 (38), 300 (36), 214 (39), 211 (37), 201 (32), 198 (30), 197 (57), 180 (100), 178 (43), 168 (73), 167 (48), 166 (41), 164 (59), 155 (58), 153 (55), 145 (52), 140 (40), 135 (54), 132 (45), 128 (64), 126 (44), 124 (86), 91 (71); Anal. calcd. for C₁₆H₁₄ClN₅O₂S (375.83): C, 51.13.62; H, 3.75; N, 18.63; Found: C, 51.40; H, 3.89; N, 18.91.

3.1.6. N-(1-(3-(2-Chlorobenzyl)-2,6-dioxo-2,3,6,7-tetrahydro-1H-purin-8-yl)-2-(4-chlorophenyl) vinyl)acetamide (5)

Yield: 64%; m.p.=260–263 °C; IR (KBr) ν_{\max} (cm⁻¹): 3294, 3178 (NH), 3070 (CH arom.), 2978 (CH aliph.), 1705, 1620, (C=O), 1566 (C=N), 1489 (C=C), 825 (*p*-substituted phenyl), 756 (*o*-substituted phenyl); ¹H NMR (DMSO-d₆): δ 12.66 (s, 1H, NH), 11.04 (s, 1H, NH), 9.48 (s, 1H, NH), 7.63–7.31 (d, *J* = 8.4 Hz, 1H, arom.), 7.52–7.50 (d, *J* = 8.8 Hz, 1H arom.), 7.41–7.39 (d, *J* = 8.8 Hz, 1H, arom.), 7.37–7.33 (m, 1H, arom.), 7.30–7.29 (m, 1H, arom.), 7.19–6.99 (m, 3H, arom.), 6.68 (s, 1H), 5.12 (s, 2H), 1.91 (s, 3H, CH₃) ppm.; ¹H NMR (DMSO-d₆): δ 168.45, 159.70, 154.46, 150.21, 148.49, 144.84, 141.15, 138.11, 136.19, 133.57, 132.11, 130.80, 129.94, 129.28, 128.04, 125.85, 125.55, 124.31, 121.86, 80.50, 43.80, 34.10 ppm; MS: *m/z* (%) = *M* + 4, 474 (32), *M* + 2, 472 (35), *M*+, 470 (52), 463 (34), 447 (41), 220 (74), 211 (68), 162 (54), 54 (100), 52 (55); Anal. calcd. for C₂₂H₁₇Cl₂N₅O₃ (470.31): C, 56.18; H, 3.64; N, 14.89.

3.1.7. 1-Substituted-6-amino-5-(4-arylidene-2-methyl)imidazolylpyrimidinediones 6-13

A mixture of 5,6-diaminouracils (0.75 mmol), the appropriate oxazole derivatives (0.75 mmol) and drops of acetic acid was heated under fusion for 5–8 min. An adequate amount of ethanol was added to the residue. The precipitate was filtered, washed with ethanol and crystallized from DMF/ethanol (2:1).

3.1.8. 6-Amino-5-(4-(4-chlorobenzylidene)-2-methyl-5-oxo-4,5-dihydro-1H-imidazol-1-yl)-1,3-dimethylpyrimidine-2,4-(1H,3H)-dione (6)

Yield: 74%; m.p. > 330 °C; IR (KBr) ν_{\max} (cm⁻¹): 3317, 3170 (NH₂), 3065 (CH arom), 2951 (CH aliph), 1712, 1674 (C=O), 1621 (C=C), 1566 (C=N); ¹H NMR (DMSO-d₆): 9.67 (s, 1H, benzylidenic), 7.93–7.90 (d, *J* = 8.0 Hz, 2H, arom.), 7.44–7.41 (d, *J* = 8.0 Hz, 2H, arom.), 7.37 (s, 2H, NH₂), 3.39 (s, 3H, CH₃), 3.16 (s, 3H, CH₃), 2.06 (s, 3H, CH₃); ¹³C NMR (DMSO-d₆): δ 160.61, 159.70, 155.14, 151.05, 150.00, 147.70, 144.97, 134.51, 131.92, 130.22, 129.32, 105.32, 31.01, 30.03, 18.44 ppm. MS: *m/z* (%) = *M* + 2, 375 (17), *M*+, 373 (29), 357 (43), 305 (18), 290 (100), 277 (35), 238 (51), 186 (74), 129 (14), 79 (23), 49 (42); Anal. calcd. for C₁₇H₁₆ClN₅O₃ (373.09): C, 54.65; H, 4.31; N, 18.74. Found: C, 54.89; H, 4.50; N, 18.95.

3.1.9. 6-Amino-1-(2-chlorobenzyl)-5-(2-methyl-4-(3-nitrobenzylidene)-5-oxo-4,5-dihydro-1H-imidazol-1-yl)pyrimidine-2,4(1H,3H)-dione (7)

Yield: 65 %; m.p.=206 °C; IR (KBr) ν_{\max} (cm⁻¹): 3340, 3201 (NH₂), 3062 (CH arom.), 2931 (CH aliph.), 1705, 1635 (C=O), 1581 (C=N), 1514 (C=C), 1512 (NO₂ asymstr), 1381 (NO₂ symstr), 771 (*m*-substituted phenyl), 748 (*o*-substituted phenyl); ¹H NMR (DMSO-d₆) δ 11.14 (s, 1H, NH, exchangeable), 9.21 (s, 1H, arom.), 8.62–8.60 (d, *J* = 8.0 Hz, 1H, arom.), 8.25–8.22 (d, *J* = 8.0 Hz, 1H, arom.), 7.78–7.74 (m, 1H, arom.), 7.53–7.51 (m, 1H, arom.), 7.41–7.7. 7.35 (m, 2H, arom. & 2H NH₂, exchangeable), 7.15 (s, 1H), 6.99–6.97 (m, 1H, arom.), 5.13 (s, 2H), 2.22 (s, 3H, CH₃); ¹³C NMR (DMSO-d₆): δ 170.66, 168.54, 159.70, 150.21, 148.49, 141.29, 139.30, 138.11, 136.36, 136.19, 133.57, 132.06, 130.00, 129.35, 127.92, 125.81, 125.72, 125.55, 124.34, 121.81, 43.84, 22.83 ppm.; MS: *m/z* (%) = *M* + 2, 482 (25), *M*+, 480 (35), 475

(30), 455 (47), 436 (46), 335 (54), 300 (40), 298 (53), 227 (56), 225 (46), 220 (100), 153 (75), 128 (79), 60 (59), 53 (98); Anal. calcd. for $C_{22}H_{17}ClN_6O_5$ (480.87): C, 54.95; H, 3.56; N, 17.48; Found: C, 55.12; H, 3.71; N, 17.69.

3.1.10. 6-Amino-1-benzyl-5-(2-methyl-4-(3-nitrobenzylidene)-5-oxo-4,5-dihydro-1H-imidazol-1-yl)pyrimidine-2,4(1H,3H)-dione (**8**)

Yield: 68%; m.p. = 178 °C; IR (KBr) ν_{\max} (cm^{-1}): 3363, 3201 (NH₂), 3070 (CH arom.), 2924 (CH aliph.), 1705, 1635, (C=O), 1573 (C=N), 1527 (C=C), 1512 (NO₂ asymstr), 1381 (NO₂ symstr), 771 (*m*-substituted phenyl); ¹H NMR (400 MHz, DMSO-*d*₆) δ 11.08 (s, 1H, NH), 9.20 (s, 1H, arom.), 8.61–8.59 (d, *J* = 7.8 Hz, 1H, arom.), 8.24–8.22 (d, *J* = 8.4 Hz, 1H, arom.), 7.76–7.68 (m, 3H, arom.), 7.38–7.23 (m, 5H, arom. & NH₂), 7.14 (s, 1H), 5.15 (s, 2H), 2.16 (s, 3H, CH₃); ¹³C NMR (DMSO-*d*₆): δ 167.59, 159.30, 153.96, 150.28, 148.14, 140.94, 137.69, 136.11, 130.24, 128.61, 128.54, 127.30, 126.27, 126.17, 125.57, 123.86, 121.21, 82.97, 44.37, 21 ppm.; MS: *m/z* (%) = *M*+, 446 (31), 442 (40), 439 (36), 431 (67), 409 (80), 480 (69), 375 (54), 366 (57), 352 (57), 348 (66), 161 (100), 77 (73); Anal. calcd. for $C_{22}H_{18}N_6O_5$ (446.42): C, 59.19; H, 4.06; N, 18.83; Found: C, 58.97; H, 4.23; N, 18.97.

3.1.11. 6-Amino-1-ethyl-5-(2-methyl-4-(3-nitrobenzylidene)-5-oxo-4,5-dihydro-1H-imidazol-1-yl)pyrimidine-2,4(1H,3H)-dione (**9**)

Yield: 89%; m.p. = 298–300 °C; IR (KBr) ν_{\max} (cm^{-1}): 3327, 3232 (NH₂), 3085 (CH arom.), 2993 (CH aliph.), 1735, 1651 (C=O), 1558 (C=N), 1473 (C=C), 1519 (NO₂ asymstr), 1388 (NO₂ symstr), 771 (*m*-substituted phenyl); ¹H NMR (DMSO-*d*₆) δ 10.95 (s, 1H, NH exchangeable), 9.20 (s, 1H, arom.), 8.60–8.58 (d, *J* = 8.0 Hz, 1H, arom.), 8.24–8.22 (dd, *J* = 8.2 Hz, 1H, arom.), 7.78–7.74 (t, *J* = 8.0 Hz, 1H, arom.), 7.28 (s, 2H, NH₂ exchangeable), 7.13 (s, 1H), 3.92–3.87 (q, *J* = 6.9 Hz, 2H), 2.14 (s, 3H, CH₃), 1.16–1.13 (t, *J* = 6.9 Hz, 3H). ¹³C NMR (DMSO-*d*₆): δ 170.14, 167.67, 159.46, 153.52, 150.05, 148.18, 141.02, 137.68, 136.04, 130.20, 125.54, 123.80, 120.89, 83.25, 37.09, 15.22, 13.00 ppm.; MS: *m/z* (%) = *M*+, 384 (24), 374 (26), 358 (48), 313 (64), 300 (78), 290 (100), 285 (48), 283 (92), 238 (73), 200 (57), 152 (52), 139 (53), 56 (66); Anal. calcd. for $C_{17}H_{16}N_6O_5$ (384.35): C, 53.12; H, 4.20; N, 21.87; Found: C, 53.41; H, 4.37; N, 21.75.

3.1.12. 6-Amino-1-benzyl-5-(4-benzylidene-2-methyl-5-oxo-4,5-dihydro-1H-imidazol-1-yl)pyrimidine-2,4(1H,3H)-dione (**10**)

Yield: 76%; m.p. = > 320 °C; IR (KBr) ν_{\max} (cm^{-1}): 3325, 3178 (NH₂), 3050 (CH arom.), 2930 (CH aliph.), 1697, 1666, (C=O), 1559 (C=N), 1496 (C=C); ¹H NMR (DMSO-*d*₆) δ 11.06 (s, 1H, NH), 8.24–8.22 (d, *J* = 7.3 Hz, 2H, arom.), 7.48–7.45 (t, *J* = 7.3 Hz, 2H, arom.), 7.42–7.36 (m, 3H, arom.), 7.31–7.24 (m, 5H, arom. & 2H NH₂), 6.95 (s, 1H), 5.14 (s, 2H), 2.12 (s, 3H, CH₃); ¹³C NMR (DMSO-*d*₆): δ 170.38, 165.56, 159.28, 153.87, 150.27, 139.16, 136.20, 134.31, 131.73, 129.77, 128.72, 128.57, 127.31, 126.16, 124.06, 83.26, 44.63, 14.88 ppm.; MS: *m/z* (%) = *M*+, 401 (35), 386 (20), 291 (40), 249 (100), 232 (80), 231 (74), 229 (57), 170 (48), 401 (35); Anal. calcd. for $C_{22}H_{19}N_5O_3$ (401.43): C, 65.83; H, 4.77; N, 17.45; Found: C, 66.04; H, 4.93; N, 17.66.

3.1.13. 6-Amino-5-(4-benzylidene-2-methyl-5-oxo-4,5-dihydro-1H-imidazol-1-yl)-1-(2-chlorobenzyl)pyrimidine-2,4(1H,3H)-dione (**11**)

Yield: 79%; m.p = 318 °C; IR (KBr) ν_{\max} (cm^{-1}): 3340, 3201 (NH₂), 3062 (CH arom.), 2931 (CH aliph.), 1705, 1635, (C=O), 1581 (C=N), 1512 (C=C), 749 (*o*-substituted phenyl); ¹H NMR (DMSO-*d*₆): δ 11.11 (s, 1H, NH), 8.25–8.23 (d, *J* = 7.3 Hz, 2H, arom.), 7.53–7.51 (dd, *J* = 7.5 Hz, 1H, arom.), 7.49–7.43 (t, *J* = 7.3 Hz, 2H, arom.), 7.41–7.36 (m, 4H, arom.), 7.34 (s, 2H), 6.96 (s, 1H), 5.13 (s, 2H), 2.17 (s, 3H, CH₃); ¹³C NMR (DMSO-*d*₆): δ 170.39, 165.65, 159.35, 154.00, 149.98, 139.21, 134.32, 133.59, 131.73, 131.67, 129.87, 129.59, 128.76, 128.72, 127.54, 125.25, 124.24, 83.41, 43.73, 15.17 ppm. MS: *m/z* (%) = *M* + 2, 437 (11), *M*+, 435 (27), 390 (16), 388 (41), 183 (59), 180 (72), 160 (29), 158 (77), 88 (55), 69 (100); Anal. calcd. for $C_{22}H_{18}ClN_5O_3$ (435.87): C, 60.62; H, 4.16; N, 16.07; Found: C, 60.85; H, 4.38; N, 16.31.

3.1.14. 6-Amino-5-(4-benzylidene-2-methyl-5-oxo-4,5-dihydro-1H-imidazol-1-yl)-1-ethylpyrimidine-2,4(1H,3H)-dione (**12**)

Yield: 86%; m.p. = 287–280 °C; IR (KBr) ν_{\max} (cm⁻¹): 3347, 3181 (NH₂), 3028 (CH arom.), 2921 (CH aliph.), 1720, 1631, (C=O), 1573 (C=N), 1513 (C=C); ¹H NMR (DMSO-d₆): δ 10.88 (s, 1H, NH), 8.25–8.23 (d, *J* = 7.3 Hz, 2H, arom.), 7.46–7.44 (t, *J* = 7.3 Hz, 2H, arom.), 7.42–7.38 (m, *J* = 7.3 Hz, 1H, arom.), 7.24 (s, 2H), 6.95 (s, 1H), 3.90–3.87 (q, *J* = 7.0 Hz, 2H), 2.09 (s, 3H), 1.16–1.12 (t, *J* = 7.0 Hz, 3H); ¹³C NMR (DMSO-d₆): δ 170.47, 165.69, 159.21, 153.53, 149.89, 139.24, 134.34, 131.72, 129.74, 128.71, 123.96, 83.26, 37.06, 15.18, 13.00 ppm. MS: *m/z* (%) = *M*+, 339 (33), 335 (28), 307 (50), 278 (76), 261 (56), 259 (78), 250 (70), 181 (100), 151 (61), 149 (58), 148 (69) 144 (55), 140 (80), 137 (65), 339 (34), 127 (53), 52 (51); Anal. calcd. for C₁₇H₁₇N₅O₃ (339.36): C, 60.17; H, 5.05; N, 20.64; Found: C, 60.43; H, 5.21; N, 20.87.

3.1.15. 6-Amino-5-(4-benzylidene-2-methyl-5-oxo-4,5-dihydro-1H-imidazol-1-yl)-1-methyl-2-thioxo-2,3-dihydropyrimidin-4(1H)-one (**13**)

Yield: 82%; m.p = 308–310 °C; IR (KBr) ν_{\max} (cm⁻¹): 3317, 3178 (NH₂), 3072 (CH arom.), 2931 (CH aliph.), 1697, 1627, (C=O), 1559 (C=N), 1496 (C=C); ¹H NMR (DMSO-d₆) δ 12.36 (s, 1H), 8.25–8.23 (d, *J* = 7.2 Hz, 2H, arom.), 7.49–7.39 (m, 3H, arom. & NH₂), 6.98 (s, 1H), 3.77 (s, 3H, CH₃), 2.13 (s, 3H, CH₃); ¹³C NMR (DMSO-d₆): δ 176.08, 170.11, 164.93, 156.80, 153.99, 139.05, 134.24, 131.78, 129.87, 128.74, 124.38, 87.85, 36.29, 15.08 ppm.; MS: *m/z* (%) = *M*+, 341 (27), 337 (43), 332 (44), 294 (40), 290 (50), 264 (66), 241 (51), 216 (41), 165 (51), 149 (48), 108 (51), 97 (93), 88 (100), 56 (80); Anal. calcd. for C₁₆H₁₅N₅O₂S (341.39): C, 56.29; H, 4.43; N, 20.51; Found: C, 56.41; H, 4.52; N, 20.68.

3.1.16. 1-Substituted-6-amino-5-((4-(dimethylamino)benzylidene)aminopyrimidindiones **14–16**

A mixture of 5,6-diaminouracils (0.75 mmol), 4-(dimethylamino)benzaldehyde (0.75 mmol) and drops of acetic acid was heated under fusion for 5–7 min. An adequate amount of ethanol was added to the residue. The precipitate was filtered, washed with ethanol and crystallized from DMF/ethanol (3:1).

3.1.17. 6-Amino-5-((4-(dimethylamino)benzylidene)amino)-1-methyl-2-thioxo-2,3-dihydropyrimidin-4(1H)-one [**44**] (**14**)

Yield: 96%; m.p. = 282–284 °C; IR (KBr) ν_{\max} (cm⁻¹): 3332, 3147 (NH₂), 3101 (CH arom.), 2939 (CH aliph.), 1643, 1589 (C=O), 1527 (C=N), 1489 (C=C), 810 (*p*-substituted phenyl); ¹H NMR (DMSO-d₆) δ 12.11 (s, 1H), 9.60 (s, 1H), 7.75–7.73 (d, *J* = 8.8 Hz, 2H, arom.), 7.28 (s, 2H), 6.74–6.72 (d, *J* = 8.9 Hz, 2H, arom.), 3.82 (s, 3H, CH₃), 2.98 (s, 6H, 2CH₃); ¹³C NMR (DMSO-d₆): δ 172.87 (C=S), 155.34, 153.49 (C=O), 153.22, 151.45, 129.07, 126.03, 111.58, 103.59, 39.82, 36.32 ppm.; MS: *m/z* (%) = *M*+, 303 (36), 283 (89), 240 (43), 232 (50), 219 (100), 217 (45), 214 (47), 183 (53), 177 (66), 104 (45), 103 (44), 90 (85), 48 (51); Anal. calcd. for C₁₄H₁₇N₅OS (303.38): C, 55.43; H, 5.65; N, 23.08; Found: C, 55.47; H, 5.84; N, 22.79.

3.1.18. 6-Amino-1-benzyl-5-((4-(dimethylamino)benzylidene)amino)pyrimidine-2,4(1H,3H)-dione (**15**)

Yield: 86%; m.p. = 270–272 °C; IR (KBr) ν_{\max} (cm⁻¹): 3356, 3163 (NH₂), 3032 (CH arom.), 2893 (CH aliph.), 1697, 1604 (C=O), 1550 (C=N), 1496 (C=C), 817 (*p*-substituted phenyl); ¹H NMR (DMSO-d₆) δ 10.79 (s, 1H), 9.55 (s, 1H), 7.68–7.66 (d, *J* = 8.9 Hz, 2H, arom.), 7.37–7.34 (t, *J* = 7.3 Hz, 2H, arom.), 7.29–7.23 (m, 3H, arom.), 7.13 (s, 2H, NH₂), 6.71–6.69 (d, *J* = 8.9 Hz, 2H, arom.), 5.19 (s, 2H), 2.95 (s, 6H.); ¹³C NMR (DMSO-d₆): δ 158.15, 153.39, 151.16, 143.26, 136.35, 128.59, 128.44, 127.21, 126.65, 126.36, 111.68, 103.68, 99.37, 44.48, 35.98 ppm.; MS: *m/z* (%) = *M*+, 363 (35), 362 (33), 342 (48), 314 (100), 313 (47), 306 (40), 302 (58), 299 (78), 297 (58), 255 (71), 177 (44), 129 (65), 104 (62), 102 (54), 60 (37), 49 (55); Anal. calcd. for C₂₀H₂₁N₅O₂ (363.42): C, 66.10; H, 5.82; N, 19.27; Found: C, 66.24; H, 5.57; N, 19.13.

3.1.19. 6-Amino-5-((4-(dimethylamino)benzylidene)amino)-1-ethylpyrimidine-2,4(1H,3H)-dione (**16**)

Yield: 78%; m.p = 280 °C; IR (KBr) ν_{\max} (cm⁻¹): 3379, 3170 (NH₂), 3024 (CH arom.), 2939 (CH aliph.), 1689, 1604 (C=O), 1543 (C=N), 1496 (C=C), 810 (*p*-substituted phenyl); ¹H NMR (DMSO-d₆): δ 10.61 (s, 1H), 9.54 (s, 1H), 7.69–7.67 (d, *J* = 8.8 Hz, 2H, arom.), 7.17 (s, 2H), 6.72–6.70 (d, *J* = 8.8 Hz, 2H, arom.), 3.94–3.92 (q, *J* = 6.9 Hz, 2H), 2.98 (s, 6H, 2CH₃), 1.16–1.13 (t, *J* = 6.9 Hz, 3H); ¹³C NMR (DMSO-d₆): δ 157.99, 152.98, 151.09, 150.70, 148.90, 128.49, 126.66, 111.70, 99.15, 36.97, 13.37, 13.10 ppm.; MS: *m/z* (%) = *M*⁺, 301 (44), 292 (34), 283 (40), 248 (39), 204 (34), 109 (37), 68 (100); Anal. calcd. for C₁₅H₁₉N₅O₂ (301.35): C, 59.79; H, 6.36; N, 23.24; Found: C, 59.93; H, 6.14; N, 23.37.

3.2. Biological Activity

3.2.1. Antibacterial and Antifungal Activity

The biological activity of the synthesized uracil derivative compounds was assessed against various antibiotic resistant bacteria such as *E. coli*, *Pseudomonas* sp., *Salmonella* sp., *S. aureus* and *Bacillus* sp., isolated from different human medical specimens (Al-Ahrar Hospital, Zagazig, Egypt). These bacterial isolates were identified based on their biochemical features according to Bergey's manual [61–63]. In addition, the activity of these compounds was evaluated against various pathogenic fungi; *A. flavus* and *C. albicans*. The antimicrobial activity of the tested compounds was determined by the disc-diffusion assay [64]. One mL of bacteria cell suspensions (10⁷ CFU/mL) from 24 h old cultures, was seeded into the nutrient agar medium, shaken vigorously then poured into sterilized Petri-dish. After medium solidification, 20 μ L of the different concentrations of the synthesized compounds were loaded into filter paper disc (8.0 mm) that placed on the plate surface, then, the cultures were incubated for 37 °C for 24 h. The experimental compounds were completely dissolved in 10% DMSO, as well as, the further dilutions were made using 10% DMSO. The solubility and stability of the synthesized compounds were assessed from the UV-Vis spectral analysis. The compounds were completely dissolved and with no signs of precipitation over 5 days at room temperature (Figure S1). After incubation, observed for the zone of inhibition and diameter of these zones were measured in millimeters. The inhibition area was calculated comparing to the total bacterial growth area using Image J software portal [65].

3.2.2. Transmission Electron Microscopic Analysis

For evaluation of the cytomorphological alterations induced by the most active compounds, the most resistant bacteria were treated with the compounds at their MIC doses, and the cellular organelles were investigated. The IC₅₀ value was expressed by the concentration of compounds inhibiting the growth of 50% of initial microbial growth, as revealed from the regression curve. The Minimum Inhibitory Concentration (MIC) was expressed by the concentration of compound preventing the visible growth of microorganism. The IC₅₀ value and MIC value of the potent compounds **3**, **12**, **13**, **14** and **16** were summarized in Table S6. The bacterial broth culture was incubated for 6 h, then amended with the tested compounds at their MIC dose, and continue for 24 h incubation at the same conditions. The bacterial cells were collected by centrifugation at 6000 rpm for 10 min, washed with sterile distilled water. The samples were prepared by immersing in primary fixative (2.5% glutaraldehyde buffered to pH 7.4 with 0.2 M phosphate buffer) for 3 h, and then post-fixed in 1 % osmium tetroxide for 2 h, buffered with the phosphate buffer for 30 min. All steps of fixation were carried out at 4 °C, the samples were dehydrated in a series of ethanol (50% to 100%), then embedded in resin capsule, that sectioned into ultrathin section of 70 nm, loaded on copper grids and contrasted with uranium acetate and lead citrate prior examination by JEOL-1200 EX microscope (National Research Centre, Giza, Egypt).

3.2.3. Cytotoxicity Assay

The cytotoxicity of the experimental compounds was evaluated towards VERO-E6 cells using the 3-(4,5-dimethylthiazol-2-yl)-2, 5-diphenyltetrazolium bromide (MTT) assay with slight modifications [64]. The stock solutions of compounds were prepared by dissolving in 10% DMSO in ddH₂O and diluted further to the working solutions with DMEM. Briefly, the cells were seeded in 96 well-plates (100 µL/well at a density of 3×10^5 cells/mL), incubated for 24 h at 37 °C in 5%CO₂, the cells were treated with various concentrations of the tested compounds in triplicates, and further incubated for 24 h. The supernatant was discarded and cell monolayers were washed with sterile phosphate buffered saline and the MTT solution (20 µL of 5 mg/mL stock solution) was added to each well and incubated at 37 °C for 4 h followed by medium aspiration. The developed formazan crystals were dissolved in 200 µL of acidified isopropanol and measured at λ_{540} nm using a multi-well plate reader. To assess the half maximal cytotoxic concentration (CC₅₀), the percentage of cytotoxicity compared to the untreated cells was determined with the following equation.

$$\% \text{ cytotoxicity} = ((\text{absorbance of cells without treatment} - \text{absorbance of cells with treatment}) \times 100) / (\text{absorbance of cells without treatment})$$

The plot of % cytotoxicity versus sample concentration was used to calculate the concentration which exhibited 50% cytotoxicity (CC₅₀).

3.3. Molecular Docking Study

The structures of all tested compounds were modeled using the Chemsketch software (<http://www.acdlabs.com/resources/freeware/> (accessed on 5 May 2021)). The structures were optimized and energy minimized using VEGAZZ software [66]. The optimized compounds were used to perform molecular docking to elucidate the anticancer activity against one fungal target protein which is acyl carrier protein domain from a fungal type I polyketide synthase (ACP), and two bacterial proteins including DNA gyrase (DNAG), and Baumannii penicillin-binding protein (PBP) to speculate the proposed antifungal and antibacterial activity for the most promising compounds. The three-dimensional structure of the molecular target was obtained from Protein Data Bank (PDB) (www.rcsb.org (accessed on 5 May 2021): (PDB: 2KR5, <https://www.rcsb.org/structure/2KR5> (accessed on 5 May 2021), (PDB: 1KZN, <https://www.rcsb.org/structure/1KZN> (accessed on 5 May 2021), and (PDB: 3UDI, <https://www.rcsb.org/structure/3UDI> (accessed on 5 May 2021) respectively. The steps for receptor preparation included the removal of heteroatoms (water and ions), the addition of polar hydrogen, and the assignment of charge. The active sites were defined using grid boxes of appropriate sizes around the bound cocrystal ligands. The docking study was performed using Autodock vina [67] and Chimera for visualization [68]. All docking procedures and scoring were recorded according to our previous publications [69–71].

Docking procedures and scoring were recorded according to established protocols [68,72–74].

3.4. Pharmacokinetics and ADME Activity

To identify the biological targets for the most promising tested compound, we employed searching in database function integrated on Swiss institute Bioinformatics tools. Further on absorption, distribution, metabolism, and excretion “ADME” were calculated hypothetically.

3.5. Computational Method

The geometric parameters and energies were computed by density functional theory at the B3LYP/CEP-31G level of theory, using the GAUSSIAN 98W package of the programs [75], on geometries that were optimized at CEP-31G basis set. The high basis set was chosen to detect the energies at a highly accurate level. The atomic charges were

computed using the natural atomic orbital populations. The B3LYP is the key word for the hybrid functional [76], which is a linear combination of the gradient functionals proposed by Becke [77] and Lee, Yang and Parr [78], together with the Hartree-Fock local exchange function [79]. UV spectra were recorded in Rigol, Ultra- 3000 series in Enzymology and Fungal Biotechnology Lab, Faculty of Science, Zagazig University.

4. Conclusions

The corresponding xanthenes **3-5**, and imidazolone derivatives **6-13**, were obtained via reaction of oxazolone derivative **2** with 5,6-diaminouracils **1** under various conditions in excellent yields. The condensation of 5,6-diaminouracils **1** with aldehyde afforded 5-Benzylideneaminouracils **14-16**. The structural identities of the resulting compounds were resolved by IR, ¹H-, ¹³C-NMR and Mass spectral analyses. The compounds **3**, **6** and **16** displayed the highest activity against *E. coli* (IC₅₀ value 1.8–1.9 µg/mL). The compound **16** displayed a significant antifungal activity against *C. albicans* (0.82 µg/mL), *A. flavus* (1.2 µg/mL) comparing to authentic antibiotics. This study paves the way for new generations of uracil and imidiazolone derivatives as potential antimicrobial and biologically active agents.

Supplementary Materials: The following data are available online <https://www.mdpi.com/article/10.3390/ijms222010979/s1>.

Author Contributions: S.E.-K. Conceived and designed the work. S.E.-K. wrote the manuscript. S.E.-K. and F.A. performed the experiments and analyzed the data. A.S.A.E.-S. perform the biological analysis, and S.E.-K. Revise the manuscript. W.A.Z. performs the DFT calculation. All authors have read and agreed to the published version of the manuscript.

Funding: The work has been funded by our own money.

Institutional Review Board Statement: Ethical review and approval were waived for this study, due to the absence of any direct work with animals or human.

Informed Consent Statement: The study does not include any experiments related to human.

Data Availability Statement: All the data are included on this manuscript as well as enclosed supplementary data.

Acknowledgments: The authors thank Ahmed Mostafa for carrying out the cytotoxicity of synthesized compounds at the Center of Scientific Excellence for Influenza viruses, National Research Center, Egypt, and Mohamed Tantawy for doing the molecular modeling (Docking) analysis for the synthesized compounds at biochemistry division, National Research Centre, El-Buhouth St., Dokki-Cairo, 12622, Egypt.

Conflicts of Interest: The authors declare no conflict of interest.

References

1. Alghamdi, S.S.; Suliman, R.S.; Almutairi, K.; Kahtani, K.; Aljatli, D. Imidazole as a Promising Medicinal Scaffold: Current Status and Future Direction. *Drug Des. Dev. Ther.* **2021**, *ume 15*, 3289–3312. [CrossRef]
2. Sherer, C.; Snape, T.J. Heterocyclic scaffolds as promising anticancer agents against tumours of the central nervous system: Exploring the scope of indole and carbazole derivatives. *Eur. J. Med. Chem.* **2015**, *97*, 552–560. [CrossRef] [PubMed]
3. Report of the WHO-China Joint Mission on Coronavirus Disease 2019 (COVID-19). Available online: <https://www.who.int/docs/default-source/coronaviruse/who-china-joint-mission-on-covid-19-final-report.pdf> (accessed on 24 February 2020).
4. Desai, N.C.; Wadekar, K.R.; Mehta, H.K.; Pandit, U.P. Design, Synthesis, and Antimicrobial Activity of Novel Fluorine-Containing Imidazolones. *Russ. J. Org. Chem.* **2021**, *57*, 976–985. [CrossRef]
5. Cassini, A.; Högberg, L.D.; Plachouras, D.; Quattrocchi, A.; Hoxha, A.; Simonsen, G.S.; Colomb-Cotinat, M.; Kretzschmar, M.E.; Devleeschauwer, B.; Cecchini, M. Attributable deaths and disability-adjusted life-years caused by infections with antibiotic-resistant bacteria in the EU and the European Economic Area in 2015: A population-level modelling analysis. *Lancet Infect. Dis.* **2019**, *19*, 56–66. [CrossRef]
6. Zhou, F.; Yu, T.; Du, R.; Fan, G.; Liu, Y.; Liu, Z.; Xiang, J.; Wang, Y.; Song, B.; Gu, X.; et al. Clinical course and risk factors for mortality of adult inpatients with COVID-19 in Wuhan, China: A retrospective cohort study. *Lancet* **2020**, *395*, 1054–1062. [CrossRef]

7. Yang, X.; Yu, Y.; Xu, J.; Shu, H.; Xia J Liu, H.; Wu, Y.; Zhang, L.; Yu, Z.; Fang, M. Clinical course and outcomes of critically ill patients with SARS-CoV-2 pneumonia in Wuhan, China: A single-centered, retrospective, observational study. *Lancet Respir. Med.* **2020**, *8*, 475–481. [[CrossRef](#)]
8. Lescure, F.-X.; Bouadma, L.; Nguyen, D.; Parisey, M.; Wicky, P.-H.; Behillil, S.; Gaymard, A.; Bouscambert-Duchamp, M.; Donati, F.; Le Hingrat, Q.; et al. Clinical and virological data of the first cases of COVID-19 in Europe: A case series. *Lancet Infect. Dis.* **2020**, *20*, 697–706. [[CrossRef](#)]
9. MacIntyre, C.R.; Chughtai, A.A.; Barnes, M.; Ridda, I.; Seale, H.; Toms, R.; Heywood, A. The role of pneumonia and secondary bacterial infection in fatal and serious outcomes of pandemic influenza a(H1N1)pdm09. *BMC Infect. Dis.* **2018**, *18*, 637. [[CrossRef](#)]
10. Molina, P.; Tárraga, A.; Otón, F. Imidazole derivatives: A comprehensive survey of their recognition properties. *Org. Biomol. Chem.* **2012**, *9*, 1711–1724. [[CrossRef](#)]
11. Sanad, S.M.H.; Mekky, A.E.M. Efficient synthesis and characterization of novel bis-heterocyclic derivatives and benzo-fused macrocycles containing oxazolone or imidazolone subunits. *J. Heterocycl. Chem.* **2020**, *57*, 3930–3942. [[CrossRef](#)]
12. Mikhaylov, A.A.; Solyev, P.N.; Kuleshov, A.V.; Kublitskii, V.S.; Korlyukov, A.A.; Lushpa, V.A.; Baranov, M.S. Imidazolone-activated donor-acceptor cyclopropanes with a peripheral stereocenter. A study on stereoselectivity of cycloaddition with aldehydes. *Chem. Heterocycl. Compd.* **2020**, *56*, 1092–1096. [[CrossRef](#)]
13. Kumar, S.; Aghara, J.C.; Manoj, A.; Alex, A.T.; Mathew, A.J.; Joesph, A. Novel Quinolone Substituted Imidazol-5(4H)-ones as Anti-inflammatory, Anticancer Agents: Synthesis, Biological Screening and Molecular Docking Studies. *Indian J. Pharm. Educ. Res.* **2020**, *54*, 771–780. [[CrossRef](#)]
14. Zaitseva, E.R.; Smirnov, A.Y.; Ivanov, I.A.; Mineev, K.S.; Baranov, M.S. Synthesis of 5-(aminomethylidene) imidazol-4-ones by using N,N-dialkylformamide acetals. *Chem. Heterocycl. Compd.* **2020**, *56*, 1097–1099. [[CrossRef](#)]
15. Snieckus, V.; Richardson, P. Synthesis of C2-Substituted Imidazolones. *Synfacts* **2020**, *16*, 1149. [[CrossRef](#)]
16. Desai, N.; Joshi, V.; Rajpara, K.; Makwana, A.H. A new synthetic approach and in vitro antimicrobial evaluation of novel imidazole incorporated 4-thiazolidinone motifs. *Arab. J. Chem.* **2017**, *10*, S589–S599. [[CrossRef](#)]
17. Shao, J.; Huang, C.H.; Shao, B.; Qin, L.; Xu, D.; Li, F.; Qu, N.; Xie, L.N.; Kalyanaraman, B.; Zhu, B.Z. Potent Oxidation of DNA by Haloquinoid Disinfection Byproducts to the More Mutagenic Imidazolone dIz via an Unprecedented Haloquinone-Enoxy Radical-Mediated Mechanism. *Environ. Sci. Technol.* **2020**, *54*, 6244. [[CrossRef](#)]
18. Abdelhameid, M.K.; Zaki, I.; Mohammed, M.R.; Mohamed, K.O. Design, synthesis, and cytotoxic screening of novel azole derivatives on hepatocellular carcinoma (HepG2 Cells). *Bioorganic Chem.* **2020**, *101*, 103995. [[CrossRef](#)]
19. Hebert, S.P.; Schlegel, H.B. Computational Investigation into the Oxidation of Guanine to Form Imidazolone (Iz) and Related Degradation Products. *Chem. Res. Toxicol.* **2020**, *33*, 1010–1027. [[CrossRef](#)]
20. Zaitseva, E.R.; Smirnov, A.Y.; Myasnyanko, I.; Sokolov, A.I.; Baranov, M.S. Synthesis of 2-arylideneimidazo [1,2-a]pyrazine-3,6,8(2H,5H,7H)-triones as a result of oxidation of 4-arylidene-2-methyl-1H-imidazol-5(4H)-ones with selenium dioxide. *Chem. Heterocycl. Compd.* **2020**, *56*, 116–119. [[CrossRef](#)]
21. Xu, B.; Lee, E.M.; Medina, A.; Sun, X.; Wang, D.; Tang, H.; Zhou, G.-C. Inhibition of zika virus infection by fused tricyclic derivatives of 1,2,4,5-tetrahydroimidazo[1,5-a]quinolin-3(3aH)-one. *Bioorganic Chem.* **2020**, *104*, 104205. [[CrossRef](#)]
22. Desai, N.C.; Vaghani, H.V.; Rajpara, K.M.; Joshi, V.V.; Satodiya, H.M. Novel approach for synthesis of potent antimicrobial hybrid molecules containing pyrimidine-based imidazole scaffolds. *Med. Chem. Res.* **2014**, *23*, 4395. [[CrossRef](#)]
23. Desai, N.C.; Vaghani, H.V.; Karkar, T.J.; Patel, B.Y.; Jadeja, K.A. Synthesis and antimicrobial studies of 1, 2, 3, 4-tetrahydropyrimidine bearing imidazole analogues. *Indian J. Chem. Sect. B* **2017**, *56*, 438.
24. Desai, N.C.; Vaja, D.V.; Jadeja, K.A.; Joshi, S.B.; Khedkar, V.M. Synthesis, Biological Evaluation and Molecular Docking Study of Pyrazole, Pyrazoline Clubbed Pyridine as Potential Antimicrobial Agents. *Anti-Infect. Agents* **2020**, *18*, 306–314. [[CrossRef](#)]
25. El-Kalyoubi, S.A.; Fayed, E.A.; Abdel-Razek, A.S. One pot synthesis, antimicrobial and antioxidant activities of fused uracils: Pyrimidodiazepines, lumazines, triazolouracil and xanthines. *Chem. Cent. J.* **2017**, *11*, 1–13. [[CrossRef](#)]
26. Singh, G.; Sharma, G.; Kalra, S.P.; Satija, P.; Singh, P.B.; Wreidt, M. Click-Derived Uracil-Appended Organosilatranyl Scaffolds: Synthesis, Antibacterial Characteristics, Pb²⁺ Binding and Fabrication of Hybrid Silica Nanoparticles. *Chem. Select.* **2020**, *5*, 284–292.
27. Hawser, S.; Lociuro, S.; Islam, K. Dihydrofolate reductase inhibitors as antibacterial agents. *Biochem. Pharmacol.* **2006**, *71*, 941–948. [[CrossRef](#)]
28. Deshmukh, M.B.; Salunkhe, S.M.; Patil, D.R.; Anbhule, P.V. A novel and efficient one step synthesis of 2-amino-5-cyano-6-hydroxy-4-aryl pyrimidines and their anti-bacterial activity. *Eur. J. Med. Chem.* **2009**, *44*, 2651–2654. [[CrossRef](#)]
29. Buron, F.; Merour, J.Y.; Akssira, M.; Guillaumet, G.; Routier, S. ChemInform Abstract: Recent Advances in the Chemistry and Biology of Pyridopyrimidines. *Angew. Chem.* **2015**, *46*, 9576–9595. [[CrossRef](#)]
30. Lu, X.; Chen, Y.; Guo, Y.; Liu, Z.; Shi, Y.; Xu, Y.; Wang, X.; Zhang, Z.; Liu, J. The design and synthesis of N-1-alkylated-5-aminoaryalkylsubstituted-6-methyluracils as potential non-nucleoside HIV-1 RT inhibitors. *Bioorganic Med. Chem.* **2007**, *15*, 7399–7407. [[CrossRef](#)]
31. Ding, Y.; Girardet, J.-L.; Smith, K.L.; Larson, G.; Prigaro, B.; Wu, J.Z.; Yao, N. Parallel synthesis of 5-cyano-6-aryl-2-thiouracil derivatives as inhibitors for hepatitis C viral NS5B RNA-dependent RNA polymerase. *Bioorganic Chem.* **2006**, *34*, 26–38. [[CrossRef](#)]

32. El-Brollosy, N.R.; Al-Deeb, O.A.; El-Emam, A.A.; Pedersen, E.B.; La Colla, P.; Collu, G.; Sanna, G.; Loddo, R. Synthesis of Novel Uracil Non-Nucleoside Derivatives as Potential Reverse Transcriptase Inhibitors of HIV-1. *Arch. Pharm.* **2009**, *342*, 663–670. [[CrossRef](#)]
33. El-Brollosy, N.R.; Al-Omar, M.A.; Al-Deeb, O.A.; El-Emam, A.A.; Nielsen, C. Synthesis of novel uracil non-nucleosides analogues of 3,4-dihydro-2-alkylthio-6-benzyl-4-oxo-pyrimidines and 6-benzyl-1-ethoxymethyl-5-isopropyluracil. *J. Chem. Res.* **2007**, *5*, 263–267. [[CrossRef](#)]
34. Nuñez, M.; Gavilan, M.D.; Conejo-García, A.; Cruz-Lopez, O.; Gallo, M.; Espinosa, A.; Campos, J. Design, Synthesis and Anticancer Activity Against the MCF-7 Cell Line of Benzo-Fused 1,4-Dihetero Seven- and Six-Membered Tethered Pyrimidines and Purines. *Curr. Med. Chem.* **2008**, *15*, 2614–2631. [[CrossRef](#)]
35. Boisdron-Celle, M.; Remaud, G.; Traore, S.; Poirier, A.L.; Gamelin, L.; Morel, A.; Gamelin, E. 5-Fluorouracil-related severe toxicity: A comparison of different methods for the pretherapeutic detection of dihydropyrimidine dehydrogenase deficiency. *Cancer Lett.* **2007**, *249*, 271–282. [[CrossRef](#)]
36. Semenov, V.E.; Voloshina, A.D.; Toroptzova, E.M.; Kulik, N.V.; Zobov, V.V.; Giniyatullin, R.K.; Mikhailov, A.S.; Nikolaev, A.E.; Akamsin, V.D.; Reznik, V.S. Antibacterial and antifungal activity of acyclic and macrocyclic uracil derivatives with quaternized nitrogen atoms in spacers. *Eur. J. Med. Chem.* **2006**, *41*, 1093–1101. [[CrossRef](#)] [[PubMed](#)]
37. Antonello, M.; Dante, R.; Silvio, M.; Gerald, B.; Giovanna, S.; Claudio, P.; Anna, T.P. Discovery of uracil-based histone deacetylase inhibitors able to reduce acquired antifungal resistance and trailing growth in *Candida albicans*. *Bioorg. Med. Chem. Lett.* **2007**, *17*, 1221–1225.
38. El-Kalyoubi, S.; Agili, F. Synthesis, In Silico Prediction and In Vitro Evaluation of Antitumor Activities of Novel Pyrido[2,3-*d*]pyrimidine, Xanthine and Lumazine Derivatives. *Molecules* **2020**, *25*, 5205. [[CrossRef](#)] [[PubMed](#)]
39. El-Kalyoubi, S.; Fayed, E. Synthesis and evaluation of antitumor activities of novel fused tri- and tetracyclic uracil derivatives. *J. Chem. Res.* **2016**, *40*, 771–777. [[CrossRef](#)]
40. El-Sayed, A.S.A.; Ali, D.M.I.; Yassin, M.A.; Zayed, R.A.; Ali, G.S. Sterol inhibitor “Fluconazole” enhance the Taxol yield and molecular expression of its encoding genes cluster from *Aspergillus flavipes*. *Process Biochem.* **2019**, *76*, 55–67. [[CrossRef](#)]
41. Phalke, P.L.; Kale, R.B.; Modhave, M.B.; Sonawane, P.S.; Khaire, S.R.; Jadhav, S.L. One pot synthesis, antimicrobial and antioxidant activities of fused uracils: Pyrimidodiazepines, lumazines, triazolouracil and xanthines. *J. Drug Deliv. Therap.* **2019**, *9*, 124–127. [[CrossRef](#)]
42. Isabella, F.S.; Marra, P.; Pedro De Castro, G.W. Amarante, Recent Advances in Azlactone Transformations. *Eur. J. Org. Chem.* **2019**, *2019*, 5829. [[CrossRef](#)]
43. Muthuboopathi, G.; Shanmugarajan, T.S. Synthesis, characterization, and biological evaluation of oxazolone analogs. *Asian J. Pharm. Clin. Res.* **2018**, *11*, 159–162.
44. Yoneda, F.; Nagamatsu, T.; Yamasaki, H. Facile and General Synthesis of 8-Substituted 2-Methylthiopurin-6-ones. *Heterocycles* **1992**, *33*, 775. [[CrossRef](#)]
45. Wang, B.; Guo, F.; Huang, C.; Zhao, H. Unraveling the iterative type I polyketide synthases hidden in *Streptomyces*. *Proc. Natl. Acad. Sci. USA* **2020**, *117*, 8449–8454. [[CrossRef](#)] [[PubMed](#)]
46. Chatterji, M.; Unniraman, S.; Mahadevan, S.; Nagaraja, V. Effect of different classes of inhibitors on DNA gyrase from *Mycobacterium smegmatis*. *J. Antimicrob. Chemother.* **2001**, *48*, 479–485. [[CrossRef](#)] [[PubMed](#)]
47. El-Sayed, A.S.A.; Mohamed, N.Z.; Safan, S.; Yassin, M.A.; Shaban, L.; Shindia, A.A.; Ali, G.S.; Sitohy, M.Z. Restoring the taxol biosynthetic machinery of *Aspergillus terreus* by *Podocarpus gracilior* pilger microbiome, with retrieving the ribosome biogenesis proteins of WD40 superfamily. *Sci. Rep.* **2019**, *9*, 11534. [[CrossRef](#)]
48. Turel, I.; Golič, L.; Bukovec, P.; Gubina, M. Antibacterial tests of Bismuth(III)–Quinolone (Ciprofloxacin, cf) compounds against *Helicobacter pylori* and some other bacteria. Crystal structure of (cfH₂)₂[Bi₂Cl₁₀]·4H₂O. *J. Inorg. Biochem.* **1998**, *71*, 53–60. [[CrossRef](#)]
49. Turel, I.; Bukovec, P.; Quirós, M. Crystal structure of ciprofloxacin hexahydrate and its characterization. *Int. J. Pharm.* **1997**, *152*, 59–65. [[CrossRef](#)]
50. Yue, Y.-F.; Sun, W.; Gao, E.-Q.; Fang, C.-J.; Xu, S.; Yan, C.-H. Syntheses and crystal structures of three Mn(II) complexes with 2-hydroxynicotinate. *Inorganica Chim. Acta* **2007**, *360*, 1466–1473. [[CrossRef](#)]
51. Top, S.; Tang, J.; Vessieres, A.; Carrez, C.; Provot, C.; Jaouen, G. Ferrocenyl hydroxytamoxifen: A prototype for a new range of oestradiol receptor site-directed cytotoxics. *Chem. Commun.* **1996**, *8*, 955–956. [[CrossRef](#)]
52. Pfaff, W.; Fischer, E.O. Zur Kristallstruktur der Di-cyclopentadienyl-Verbindungen des zweiwertigen Eisens, Kobalts und Nickels. *Z. Anorg. Allg. Chem.* **1953**, *274*, 316–322. [[CrossRef](#)]
53. Becka, M.; Vilková, M.; Soral, M.; Potocnak, I.; Breza, M.; Beres, T.; Imrich, J. Synthesis and isomerisation of acridin substituted 1,3-thiazolidin-4-ones and 4-oxo-1,3-thiazolidin-5-ylidene acetates. An experimental and computational study. *J. Mol. Struct.* **2018**, *1154*, 152–164. [[CrossRef](#)]
54. Fleming, I. *Frontier Orbitals and Organic Chemical Reactions*; Wiley: London, UK, 2011.
55. Kurtaran, R.; Odabasoglu, S.; Azizoglu, A.; Kara, H.; Atako, O.L. Experimental and computational study on [2,6-bis(3,5-dimethyl-N-pyrazolyl)pyridine]-(dithiocyanato)mercury(II). *Polyhedron* **2007**, *26*, 5069–5074. [[CrossRef](#)]
56. El-Sayed, A.S.A.; Ali, G.S. *Aspergillus flavipes* is a novel efficient biocontrol agent of *Phytophthora parasitica*. *Biol. Control.* **2020**, *140*, 104072. [[CrossRef](#)]

57. Ciofini, I.; Lainé, P.P.; Bedioui, F.; Adamo, C. Photoinduced Intramolecular Electron Transfer in Ruthenium and Osmium Polyads: Insights from Theory. *J. Am. Chem. Soc.* **2004**, *126*, 10763–10777. [[CrossRef](#)] [[PubMed](#)]
58. Ciofini, I.; Daul, C.; Adam, J. Phototriggered Linkage Isomerization in Ruthenium–Dimethylsulfoxide Complexes: Insights from Theory. *J. Phys. Chem. A* **2003**, *107*, 11182–11190. [[CrossRef](#)]
59. El Baz, A.F.; Shetaia, Y.M.; Elkhoul, R.R. Xylitol production by *Candida tropicalis* under different statistically optimized growth conditions. *Afr. J. Biotechnol.* **2011**, *10*, 16617–16625. [[CrossRef](#)]
60. Bauernschmitt, R.; Ahlrichs, R. Treatment of electronic excitations within the adiabatic approximation of time dependent density functional theory. *Chem. Phys. Lett.* **1996**, *256*, 454–464. [[CrossRef](#)]
61. El-Sayed, A.S.A.; Shindia, A.A.; Zeid, A.A.A.; Yassin, A.M.; Sitohy, M.Z.; Sitohy, B. *Aspergillus nidulans* thermostable arginine deiminase-Dextran conjugates with enhanced molecular stability, proteolytic resistance, pharmacokinetic properties and anticancer activity. *Enzym. Microb. Technol.* **2019**, *131*, 109432. [[CrossRef](#)]
62. Bergey, D.H.; Bergey's, J.G.H. *Manual of Determinative Bacteriology*, 9th ed.; Williams & Wilkins: Baltimore, MD, USA, 1994.
63. Hassan, A.; Sorour, N.M.; El-Baz, A.; Shetaia, Y. Simple synthesis of bacterial cellulose/magnetite nanoparticles composite for the removal of antimony from aqueous solution. *Int. J. Environ. Sci. Technol.* **2019**, *16*, 1433–1448. [[CrossRef](#)]
64. El-Sayed, A.S.A.; Abdel-Azeim, S.; Ibrahim, H.M.; Yassin, M.A.; Abdel-Ghany, S.E.; Esener, S.; Ali, G.S. Biochemical stability and molecular dynamic characterization of *Aspergillus fumigatus* cystathionine γ -lyase in response to various reaction effectors. *Enzym. Microb. Technol.* **2015**, *81*, 31–46. [[CrossRef](#)]
65. El-Sayed, A.S.A.; Akbar, A.; Iqar, I.; Ali, R.; Norman, D.; Brennan, M.; Ali, G.S. A glucanolytic *Pseudomonas* sp. associated with *Smilax bona-nox* L. displays strong activity against *Phytophthora parasitica*. *Microbiol. Res.* **2018**, *207*, 140–152. [[CrossRef](#)]
66. Pedretti, A.; Villa, L.; Vistoli, G. VEGA – An open platform to develop chemo-bio-informatics applications, using plug-in architecture and script programming. *J. Comput. Mol. Des.* **2004**, *18*, 167–173. [[CrossRef](#)]
67. Trott, O.; Olson, A.J. AutoDock Vina: Improving the speed and accuracy of docking with a new scoring function, efficient optimization, and multithreading. *J. Comput. Chem.* **2010**, *31*, 455–461. [[CrossRef](#)]
68. Pettersen, E.F.; Goddard, T.D.; Huang, C.C.; Couch, G.S.; Greenblatt, D.M.; Meng, E.C.; Ferrin, T.E. UCSF Chimera—a visualization system for exploratory research and analysis. *J. Comput. Chem.* **2004**, *25*, 1605–1612. [[CrossRef](#)]
69. Kattan, S.W.; Nafie, M.S.; Elmgeed, G.A.; Alelwani, W.; Badar, M.; Tantawy, M.A. Molecular docking, anti-proliferative activity and induction of apoptosis in human liver cancer cells treated with androstane derivatives: Implication of PI3K/AKT/mTOR pathway. *J. Steroid Biochem. Mol. Biol.* **2020**, *198*, 105604. [[CrossRef](#)] [[PubMed](#)]
70. Tantawy, M.A.; Sroor, F.M.; Mohamed, M.F.; El-Naggar, M.E.; Saleh, F.M.; Hassaneen, H.M.; Abdelhamid, I.A. Molecular Docking Study, Cytotoxicity, Cell Cycle Arrest and Apoptotic Induction of Novel Chalcones Incorporating Thiadiazolyl Isoquinoline in Cervical Cancer. *Anti-Cancer Agents Med. Chem.* **2020**, *20*, 70–83. [[CrossRef](#)] [[PubMed](#)]
71. Nafie, M.S.; Tantawy, M.A.; Elmgeed, G.A. Screening of different drug design tools to predict the mode of action of steroidal derivatives as anti-cancer agents. *Steroids* **2019**, *152*, 108485. [[CrossRef](#)] [[PubMed](#)]
72. Abdel-Motaal, M.; Almohawes, K.; Tantawy, M.A. Antimicrobial evaluation and docking study of some new substituted benzimidazole-2yl derivatives. *Bioorganic Chem.* **2020**, *101*, 103972. [[CrossRef](#)]
73. Nagy, M.; Darwish, K.; Kishk, S.; Tantawy, M.; Nasr, A.; Qushawy, M.; Swidan, S.; Mostafa, S.; Salama, I. Design, Synthesis, Anticancer Activity, and Solid Lipid Nanoparticle Formulation of Indole- and Benzimidazole-Based Compounds as Pro-Apoptotic Agents Targeting Bcl-2 Protein. *Pharmaceuticals* **2021**, *14*, 113. [[CrossRef](#)]
74. Alsayed, M.; El-Kady, D.S.; ATantawy, M.; Abdelhalim, M.M.; Elazabawy, S.R.; Abdallah, A.E.M.; AElmegeed, G. Novel Melatonin Derivatives: Synthesis, Anticancer Evaluations and Molecular-Docking Study. *Egypt. J. Chem.* **2020**, *64*, 1517–1533. [[CrossRef](#)]
75. Frisch, M.J. *Gaussian 98, Revision A.9*; Gaussian INC.: Pittsburgh, PA, USA, 1998.
76. El-Baz, A.F.; Sorour, N.M.; Shetaia, Y.M. *Trichosporon jirovecii*-mediated synthesis of cadmium sulfide nanoparticles. *J. Basic Microbiol.* **2016**, *56*, 520–530. [[CrossRef](#)] [[PubMed](#)]
77. Becke, A.D. Density-functional exchange-energy approximation with correct asymptotic behavior. *Phys. Rev. A* **1988**, *38*, 3098–3100. [[CrossRef](#)] [[PubMed](#)]
78. Lee, C.; Yang, W.; Parr, R.G. Development of the Colle-Salvetti correlation-energy formula into a functional of the electron density. *Phys. Rev. B* **1988**, *37*, 785–789. [[CrossRef](#)]
79. Flurry, R.L., Jr. *Molecular Orbital Theory of Bonding in Organic Molecules*; Marcel Dekker: New York, NY, USA, 1968.